# Formation of Complex Molecules in Prestellar Cores: A Multilayer Approach

A. Vasyunin, P. Caselli, F. Dulieu, I. Jimenez-Serra

The Astrophysical Journal, 842:33 (18pp), 2017 June 10 https://doi.org/10.3847/1538-4357/aa72ec


# Formation of Complex Molecules in Prestellar Cores: A Multilayer Approach

A. I. Vasyunin[1,2], P. Caselli[1], F. Dulieu[3], and I. Jiménez-Serra[4]
[1] Max-Planck-Institute for Extraterrestrial Physics, Garching, Germany; anton.vasyunin@gmail.com
[2] Ural Federal University, Ekaterinburg, Russia
[3] LERMA, Université de Cergy Pontoise, Sorbonne Universités, UPMC Univ. Paris 6, PSL Research University, Observatoire de Paris, UMR 8112 CNRS, 5 mail Gay Lussac F-95000 Cergy Pontoise, France
[4] Queen Mary University, London, UK
*Received 2016 September 27; revised 2017 May 11; accepted 2017 May 12; published 2017 June 9*

## Abstract

We present the results of chemical modeling of complex organic molecules (COMs) under conditions typical for prestellar cores. We utilize an advanced gas-grain astrochemical model with updated gas-phase chemistry, with a multilayer approach to ice-surface chemistry and an up-to-date treatment of reactive desorption (RD) based on recent experiments of Minissale et al. With the chemical model, radial profiles of molecules, including COMs, are calculated for the case of the prototypical prestellar core L1544 at the timescales when the modeled depletion factor of CO becomes equal to that observed. We find that COMs can be formed efficiently in L1544 up to the fractional abundances of $10(-10)$ wrt. total hydrogen nuclei. Abundances of many COMs such as $CH_3OCH_3$, $HCOOCH_3$, and others peak at similar radial distances of 2000–4000 au. Gas-phase abundances of COMs depend on the efficiency of RD, which in turn depends on the composition of the outer monolayers of icy mantles. In prestellar cores, the outer monolayers of mantles likely include large fractions of CO and its hydrogenation products, which may increase the efficiency of RD according to Minissale et al., and makes the formation of COMs efficient under conditions typical for prestellar cores, though this assumption is yet to be confirmed experimentally. The hydroxyl radical (OH) appears to play an important role in gas-phase chemistry of COMs, which makes it deserving of further detailed studies.

*Key words:* astrochemistry – ISM: abundances – ISM: clouds – ISM: molecules – molecular processes – stars: formation

## 1. Introduction

Evolution of organic matter and build-up of molecular complexity during the process of star and planet formation is one of the most important but still not well understood questions in astochemistry (Herbst & van Dishoeck 2009). While the formation of exotic "carbon-chain" molecules known in cold interstellar cores for several decades can be explained via gas-phase ion-molecular and neutral–neutral reactions, the mechanisms of formation of saturated complex organic molecules (COMs) such as $CH_3OH$, $CH_3OCH_3$, $HCOOCH_3$, and others are more uncertain. Formation of COMs in hot cores and corinos is reasonably well explained by the "warm-up scenario" (Garrod & Herbst 2006; Garrod et al. 2008), in which COMs first form via surface radical–radical reactions at 30–40 K and then evaporate to the gas at higher temperatures reaching fractional abundances of about $\sim 10^{-8}$–$10^{-7}$ with respect to hydrogen similar to those observed (Blake et al. 1987; Cazaux et al. 2003; Bottinelli et al. 2004a, 2004b). However, organic molecules in cold cores (e.g., Öberg et al. 2010; Bacmann et al. 2012; Cernicharo et al. 2012; Vastel et al. 2014) require other mechanisms to explain their formation, since warm-up develops in later stages, after the switch on of a protostar.

To date, several scenarios have been proposed to explain the formation of COMs typical for terrestrial chemistry during the earliest stages of star formation prior to the warm-up phase. Note that all of them involve grain-surface chemical processes and non-thermal desorption of species from cold dust grains into the gas phase. The first attempt to explain terrestrial-type COMs discovered in L1689b and B1-b was made by Vasyunin & Herbst (2013b). In that study, the authors proposed that COMs in the cold gas may be formed via ion-molecule and radiative association reactions between precursor molecules formed on cold grains and then ejected in the gas phase via efficient reactive desorption (RD). While the observed abundances of COMs were satisfactorily explained, the model significantly overestimated abundances of $CH_3OH$ and $H_2CO$ in the gas phase. Balucani et al. (2015) improved this scenario by adding a neutral–neutral reaction linking methyl formate and dimethyl ether in the gas phase, and adjusting rates of several other important gas-phase reactions. These improvements allowed Balucani et al. (2015) to reach better agreement with observations for methanol and establish a clear chemical link between $CH_3OCH_3$ and $HCOOCH_3$. Reboussin et al. (2014) showed that impulsive heating of interstellar grains via cosmic-ray particles may increase the mobility of species on grain surface and enhance formation of COMs, making their abundances somewhat closer to observed values. However, Reboussin et al. (2014) do not take into account the locality of cosmic-ray heating of a dust grain and icy mantle, which has been shown to have a major effect on the chemistry in the ice (Ivlev et al. 2015). Recently, Ruaud et al. (2015) showed that the Eley–Rideal surface reaction mechanism, which does not require surface mobility of species, and is normally not considered in astrochemical models, assisted by complex induced reactions may be efficient in producing observed amounts of COMs at 10 K. However, the abundances of some important COMs such as methyl formate are below observed values by one to two orders of magnitude. Using microscopic Monte-Carlo simulations, Chang & Herbst (2016) showed that non-diffusive chain chemical reactions may lead to the formation of COMs in icy mantles of interstellar grains at low temperatures of $\sim$10 K. However, we note that the ejection

of COMs from the grain surface to the gas phase does not consider the results from recent laboratory experiments (see below, and Dulieu et al. 2013 and Minissale et al. 2016a).

Although models published to date have shed some light on the mystery of the low-temperature formation of COMs, they rely on poorly known assumptions and parameters. At low temperatures of about 10 K, the only way to establish the required feedback from grain-surface chemistry to the gas phase chemistry is to invoke non-thermal desorption of species. Under the conditions typical for cold dark clouds, the most efficient type of non-thermal desorption is likely the so-called RD (a.k.a. chemical desorption, or desorption upon formation; Garrod et al. 2006, 2007). By RD we call the process of breaking the surface-molecular bond of a reaction product due to the release of formation energy in surface two-body association reaction. RD is a complex process that is controlled by a number of factors, e.g., internal structure of molecules, type of surface, etc. The efficiency of RD (fraction of products of a surface reaction ejected into the gas phase) is a matter of debate in the community and a subject of both experimental and theoretical studies. In the early theoretical study by Garrod et al. (2007) based on Rice–Ramsperger–Kessel theory, the authors proposed the efficiency of RD to be of about 1%–3% and only slightly dependent on the type of desorbing molecule. Vasyunin & Herbst (2013b) showed that for the explanation of observed abundances of COMs in cold clouds one needs to assume efficiency of RD of about 10% at least for methanol and formaldehyde.

In a series of laboratory experiments on RD, which are the most comprehensive to date, Dulieu et al. (2013) and Minissale & Dulieu (2014) found surprisingly high efficiency of RD for certain systems (e.g., 80% for the reaction $O + O \rightarrow O_2$ on bare silicate) but also strong dependence of desorption efficiency on the particular chemical reaction and the type of surface. One of the important results for astrochemistry is that the efficiency of RD in laboratory experiments is dramatically reduced if bare silicate is covered by water ice. As summarized in Minissale et al. (2016b), for the majority of studied reactions, the efficiency of RD falls below the upper limit of 5%–10% measurable in experiments, if the surface is amorphous solid water. Using the experimental data, Minissale et al. (2016b) derived a semi-empirical theory that describes the dependence of the efficiency of RD on the type of surface, enthalpy of reaction and internal structure of desorbing molecule. The theory predicts negligible efficiency of RD for methanol and formaldehyde from the surface of water ice, which is believed to be the dominant constituent of icy mantles of grains in cold clouds (e.g., Öberg et al. 2011). This fact can be considered as a serious argument against the scenario of formation of COMs in cold clouds proposed by Vasyunin & Herbst (2013b).

However, water ice is not the only major constituent of icy mantles in cold clouds. A number of observations over the last four decades revealed the main constituents of interstellar ices to be water (Gillett & Forrest 1973), carbon monoxide (Lacy et al. 1984), carbon dioxide (de Graauw et al. 1996), methanol (Grim et al. 1991), ammonia (van Dishoeck 2004) and methane (Lacy et al. 1991). The ice composition appears to be somewhat different in protostellar objects at different stages of development, but surprisingly similar between objects from the same evolutionary class (Öberg et al. 2011). In particular, the fraction of solid CO in ice is lower in high-mass protostars (∼0.1), and significantly higher toward low-mass protostars, or prestellar cores (∼0.3; see Table 2 in Öberg et al. 2011). From the analysis of the shapes of IR absorption bands, constraints on the ice structure were also inferred. In quiescent molecular dark clouds, e.g., in prestellar cores, icy mantles likely consist of two phases: water-rich polar phase and water-poor but CO-rich apolar phase (Tielens et al. 1991). It is likely that the CO-rich apolar phase is on top of water-rich mantles, because it is mainly formed from CO accreted from the dense gas after dense clouds are formed. Observed large (⩾90%) depletion of gas-phase CO in prestellar cores (e.g., Caselli et al. 1999) and results of multilayer modeling of icy mantles (Garrod & Pauly 2011; Vasyunin & Herbst 2013a) are in favor of this assumption. As such, it is likely that the ice surface in prestellar clouds is mostly covered by CO ice, and, probably, by the product of CO hydrogenation such as formaldehyde and methanol. Indeed, Bizzocchi et al. (2014) showed that the observed methanol toward the prestellar core L1544 exhibits a low degree of deuteration compared to $N_2H^+$ and $NH_3$, which implies that its emission comes from the outer parts of the cloud where CO is on the onset of depletion. The $CH_3OH$ map obtained by these authors toward L1544 shows a ring-like structure surrounding the dust continuum emission, which peaks at a distance similar to where CO depletion occurs within the core. As such, it is likely that CO accretion onto ices and the formation of $CH_3OH$ and other COMs happens simultaneously, dominating the outer shells of icy mantles. This is in line with the recent results of Jiménez-Serra et al. (2016) who have shown that COMs are enhanced toward this $CH_3OH$-rich, ring-like structure in L1544 with respect to its center. Efficiencies of RD from CO ice have not been studied experimentally so far. However, according to the semi-empirical theory by Minissale et al. (2016b), they must be significantly higher than in the case of water ice. This makes prestellar cores excellent laboratories in which to test whether the formation of COMs in cold objects occurs via the scenario proposed by Vasyunin & Herbst (2013b).

In this work, we present an extended model of formation of COMs in prestellar cores. The model by Vasyunin & Herbst (2013b) is improved by adding a state-of-the-art treatment of RD by Minissale et al. (2016b). For the first time, we theoretically explore the impact of the composition of ice surface on the efficiency of RD and, thus, on the formation of COMs. To better treat the composition of the surface and interior (bulk) of thick icy mantles of interstellar grains in dark clouds, we employ a multilayer approach to grain-surface chemistry, and treat grain-surface and bulk chemistry separately. In addition, we consider the impact of new gas-phase reactions recently proposed by Shannon et al. (2013, 2014) and Balucani et al. (2015) on the formation of COMs. By combining our chemical model with the physical model of the prestellar core L1544 by Keto & Caselli (2010), we predict radial abundance profiles for COMs across this prototypical object.

The paper is organized as follows. In Section 2, we describe our chemical model and employ the physical model of the prestellar core L1544. In Section 3, modeling results are presented. Section 4 is devoted to the comparison with available observational data and discussion. Finally, in Section 5, the summary of the study is given.

## 2. Chemical and Physical Models

### 2.1. A Three-phase Code with Bulk Chemistry

In cold dark clouds, the thickness of icy mantles on interstellar grains is significant, and reach up to several hundreds of monolayers (e.g., Gibb et al. 2004; Garrod & Pauly 2011; Vasyunin & Herbst 2013a). The formation of such thick mantles occurs on a timescale of at least several hundred thousand years (Garrod & Pauly 2011; Vasyunin & Herbst 2013a) and happens in parallel with ongoing physical evolution of a prestellar core. As such, it is likely that the composition of ice surface and outer layers of icy mantles is different from its bulk composition. Since one of the main goals of this study is to investigate the impact of the surface composition of icy mantles on the formation of COMs in prestellar clouds, it is reasonable to employ a multilayer approach to ice chemistry. This allows us to study the composition of icy mantle surfaces explicitly, and discriminate between the chemistry that occurs on the surface and in the bulk of ice. This approach is qualitatively similar to that described by, e.g., Taquet et al. (2012), Garrod (2013), and Ruaud et al. (2016).

For this study, we modified the chemical code utilized in Vasyunin & Herbst (2013b). The code is based on chemical rate equations for gas phase chemical reactions and modified rate equations (Garrod 2008; Garrod et al. 2009) for chemical reactions in icy mantles of interstellar grains. The evolution of abundances of gas-phase species is governed by the equation

$$\frac{dn_i^{\rm gas}}{dt} = \sum_{jk} k_{jk} n_j^{\rm gas} n_k^{\rm gas} - n_i^{\rm gas} \sum_{il} k_{il} n_l^{\rm gas} - k_{\rm acc} n_i^{\rm gas} + R_i^{\rm des}, \quad (1)$$

where $n_{i(j,k)}^{\rm gas}$ is the abundance of the $i(j, k)$-th species in the gas phase, $k_{jk}$ and $k_{il}$ are the rate constants of gas-phase reactions, $k_{\rm acc}$ is the rate constant for accretion of the $i$th species to grain surface, and $R_i^{\rm des}$ is the rate of desorption of the $i$th species from grains to the gas.

The equations governing the chemistry on interstellar grains are constructed in a way to take into account the complex structure of icy mantles. The following assumptions are made. In the icy mantle, two chemically distinct phases can be picked out: surface and bulk. In both phases, chemical reactions may occur. Species can be transferred between surface and bulk when the total number of molecules in the icy mantle is changed due to accretion or desorption or, alternatively, due to thermal diffusion of molecules in the mantle. The difference between the surface and the bulk is twofold. First, desorption of species to the gas phase is only allowed from the surface, i.e., a bulk species must appear on the surface of icy mantles before desorption. Second, diffusion of species on the surface is much faster than inside the bulk. Garrod (2013) proposed that diffusion energy of species in the bulk is twice higher than on the surface. In this work, we utilize that value. The following pair of equations describes the chemical evolution of the $i$th species in the icy mantle of an interstellar grain under the above assumptions:

$$\frac{dn_i^{\rm surf}}{dt} = \left(\frac{dn_i^{\rm surf}}{dt}\right)^{\rm chem} + \left(\frac{dn_i^{\rm surf}}{dt}\right)^{\rm tran} + \left(\frac{dn_i^{\rm bulk}}{dt}\right)^{\rm diff} \quad (2)$$

$$\frac{dn_i^{\rm bulk}}{dt} = \left(\frac{dn_i^{\rm bulk}}{dt}\right)^{\rm chem} - \left(\frac{dn_i^{\rm surf}}{dt}\right)^{\rm tran} - \left(\frac{dn_i^{\rm bulk}}{dt}\right)^{\rm diff} \quad (3)$$

In Equations (2) and (3), the first term describes the evolution of the abundance of the $i$th species due to chemical reactions. In Equation (2), the first term also includes processes of accretion and desorption. This term can be expressed either as a rate equation similar to that constructed for a gas-phase species, or as a modified version of a rate equation that is capable to take into account stochastic effects in surface chemistry (Garrod 2008). Although the developed code is capable of using both types of equations, below we use modified rate equations for surface chemistry, unless otherwise stated. As shown in Garrod et al. (2009), in contrast to standard rate equations, modified rate equations produce numerical results close to those obtained with the rigorous Monte Carlo approach even in the case of the accretion-limited regime of surface chemistry at which stochastic effects are important. This regime is likely to be in action in this study due to the adopted parameters of surface chemistry (tunneling for H and $H_2$, see below).

The second term in Equations (2) and (3) is the rate of transfer of species between the surface and the bulk due to processes of accretion and desorption or change in number of molecules on the surface due to chemical reactions, i.e., due to the processes that deposit or physically remove species to/from the icy mantle. In other words, this term represents the instant change of what is surface and what is bulk of the ice rather than the physical transfer of the material in the icy mantle. This term is defined in a way similar to that in previously developed models of, e.g., Hasegawa & Herbst (1993) and Garrod & Pauly (2011):

$$\left(\frac{dn_i^{\rm surf}}{dt}\right)^{\rm tran} = \frac{n_i}{N^{\rm surf}} \cdot \left(\frac{dN^{\rm surf}}{dt}\right)^{\rm chem} \cdot \alpha_{\rm tran}. \quad (4)$$

Here, $N^{\rm surf} = \sum_i n_i$ is the total number of particles of species on the ice surface,

$$\left(\frac{dN^{\rm surf}}{dt}\right)^{\rm chem} = \sum_i \left(\frac{dn_i^{\rm surf}}{dt}\right)^{\rm chem} \quad (5)$$

is the net rate of change of the total number of particles on the surface due to chemical reactions, accretion and desorption. Note that by varying $N^{\rm surf}$, we can change the number of upper monolayers of the ice that belong to the virtual "surface" in our model. This could be necessary to better satisfy experimental data, e.g., on desorption. Following finding of Vasyunin & Herbst (2013a), we set $N^{\rm surf}$ equal to four times the number of surface binding sites, thus assigning the upper four monolayers to the "surface," or the most chemically active fraction of ice.

The last term in Equations (2) and (3) describes the real transfer of species between bulk and surface due to diffusion. In a thick mantle consisting of several hundreds of monolayers, an average atom or molecule must perform a series of jumps before reaching the surface due to 3D brownian motion. On each jump, a species has a chance to react with another reactive species or dissociate due to impact with a cosmic-ray or photon absorption. As such, the surface is only reached by those species that do not undergo any chemical transformation on its way to the surface.

Garrod (2013) defines the rate of diffusion of a species from bulk to surface with his Equation (3). Essentially, his definition assumes that any atom or molecule can reach the surface of the ice in one jump, regardless of its initial position in the mantle. We believe that it is a too optimistic estimation, since it assumes that in a series of intramantle swaps needed for a species to reach the surface, no encounter with reactive species that would lead to a chemical reaction that will eliminate a swapping species will happen. Thus, the probability that the species will reach the ice surface rather than undergo a chemical reaction inside the bulk is $(1-P)^N$, where $P$ is the probability for a species to react on a single swap and $N$ is the number of swaps needed to reach the surface. Observational data on ice composition (e.g., Öberg et al. 2011) imply that the fraction of chemically active species such as CO that can react with the most mobile species (e.g., atomic hydrogen) is tenths of percents. Assuming efficient tunneling through activation barriers of surface reactions, including that with CO (Hasegawa et al. 1992), one can roughly assume that the swapping species can undergo a chemical reaction on each swap with a probability of 25%, based on the average fraction of reactive species (mainly CO and $H_2CO$) obtained from ice observations (Öberg et al. 2011); thus we get the probability of a species to reach the surface from the layers beneath the tenth below 5%, e.g., $(1–0.25)^{11} = 0.042$. Thus, we assume that species that start to migrate from deeper positions have a negligible probability to reach the surface when compared to the probability to undergo intra-bulk chemical reactions. As such, the diffusion rate from bulk to surface (b2s) is defined as

$$R_{\mathrm{diff},b2s} = n_i^{\mathrm{bulk}} \cdot \frac{N^{\mathrm{surf}}}{N^{\mathrm{bulk}}} \cdot k_i^{\mathrm{swap}} \cdot \max\left(1, \frac{10}{N_{ml}}\right) \quad (6)$$

where $N^{\mathrm{bulk}}$ is a total number of molecules in the bulk of ice, and $k_i^{\mathrm{swap}}$ is the rate of swapping of a species in the bulk of ice, defined in the same way as in Garrod (2013), i.e., twice the surface diffusion rate of a species, $N_{ml}$ is the current number of monolayers in the mantle.

Photochemistry and chemistry induced by direct cosmic-ray impacts are treated in the same way both on surface and in the bulk of ice, and is cloned from gas-phase processes included in the model. Although it is clearly a simplification of real physical processes (see, e.g., Fayolle et al. 2011; Muñoz Caro et al. 2014; Ivlev et al. 2015), we prefer this basic approach due to the lack of experimental data on details of surface photochemistry. Five types of desorption processes are included in the model: thermal desorption, cosmic-ray-induced desorption (Hasegawa & Herbst 1993), cosmic-ray-induced photodesorption (Prasad & Tarafdar 1983), photodesorption, and reactive (or chemical) desorption. Note that the efficiency of photodesorption in releasing the methanol from icy mantles of grains to the gas phase in the outer shells of prestellar cores, is quite uncertain. Although experiments by Öberg et al. (2009) showed high efficiency of photodesorption with a yield of $10^{-3}$ molecule per incident photon, newer experiments by Bertin et al. (2016) and Cruz-Diaz et al. (2016) suggest that, at least for methanol, the yield does not exceed $10^{-5}$ molecule per incident photon, thus making the photodesorption process less efficient than, e.g., ice sputtering by cosmic rays, as shown by Dartois et al. (2015). Given the discrepancy between the old and new experimental results, in the current study we assumed a photodesorption yield equal to $10^{-5}$ molecule per incident photon.

### 2.2. Surface Formation of Methanol and Formaldehyde

The network of surface reactions used in this work is taken from Vasyunin & Herbst (2013b). In this network, formaldehyde and methanol are formed on the surface via the hydrogenation of the CO molecule in the sequence $CO \rightarrow HCO \rightarrow H_2CO \rightarrow CH_2OH \rightarrow CH_3OH$, which was experimentally confirmed by, e.g., Fuchs et al. (2009). Hydrogen addition reactions leading to the formation of HCO and $CH_2OH$ have activation barriers of 2500 K (Ruffle & Herbst 2001; see below Section 2.5 for the discussion on the shape of the reaction activation barriers). Note that this hydrogenation sequence of CO forming formaldehyde and methanol may not reflect the actual complexity of the CO hydrogenation process. Recently, Minissale et al. (2016c) showed that hydrogenation of HCO and $H_2CO$ is a more complex process accompanied by "backward" $H_2$ abstraction reactions $H + HCO \rightarrow CO + H_2$ and $H + H_2CO \rightarrow HCO + H_2$. These processes may increase the efficiency of the RD of CO and suppress the formation of methanol. Although these newly introduced processes may be of importance for the formation of COMs in cold clouds, they are not included in the present study. Branching ratios between H abstraction and H addition reactions have not yet been measured accurately (Minissale et al. 2016c). Thus, the incorporation of abstraction reactions with poorly known rates will not reduce the resulting uncertainty of our model. Mechanism of surface formation of methanol is a problem of fundamental importance in astrochemistry. A separate study must be devoted to its reconsideration.

### 2.3. Treatment of RD

The treatment of desorption in our three-phase model is similar to that described in Vasyunin & Herbst (2013b) with the exception of RD. For this type of desorption, we adopt the recent results by Minissale et al. (2016b). They derived a semi-empirical formula that describes the dependence of the efficiency of RD on the surface composition, exothermicity of a surface reaction and binding energies of reaction products:

$$R_{\mathrm{RD}} = \exp\left(-\epsilon \frac{E_b \times DF}{\Delta H}\right), \ \epsilon = \left(\frac{m-M}{m+M}\right)^2. \quad (7)$$

Here, $R_{\mathrm{RD}}$ is the efficiency of RD, i.e., the fraction of products of a surface reaction directly ejected to the gas, $E_b$ is the binding energy of a species, $DF$ is the number of vibrational modes in a molecule–surface bond system, $\epsilon$ is the fraction of kinetic energy retained by the reaction product with the mass $m$ colliding with the surface element with effective mass $M$. Experiments on scattering of molecules on surface (Hayes et al. 2012) showed that upon collision, molecules interact with a surface structural element consisting of several atoms or molecules forming the surface, not with a single one. This is due to collective effects caused by the surface rigidity. As such, the effective mass of the surface element $M$ is typically much higher than the mass of single atoms or molecules that the surface consists of.

Formula (7) has been established for rigid surface (graphite), where an effective mass has been measured by other experimental methods to be close to 1.8 masses of graphite carbon ring ($M \approx 130$ a.m.u.; see the discussion in Minissale & Dulieu 2014). Application of formula (7) for molecular surfaces also requires the assignment of a collective mass

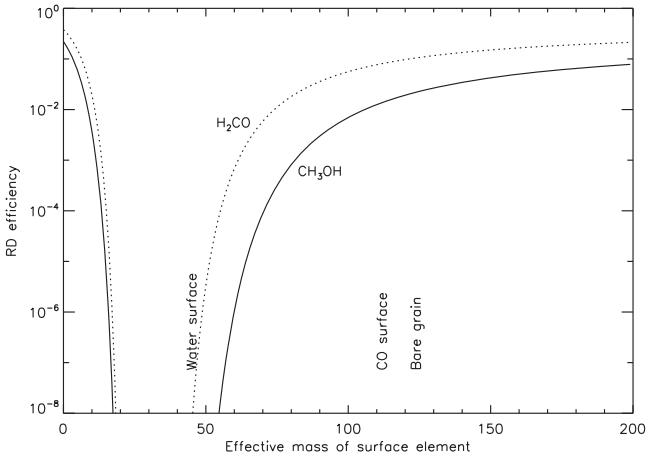


**Figure 1.** Dependence of the efficiency of reactive desorption of methanol and formaldehyde in reactions H + HCO → $H_2CO$ and H + $H_3CO$ → $CH_3OH$ on the chosen effective mass of the surface element (based on Minissale et al. (2016a); see the text for details).

larger than the individual molecule's constituent of the ice, because, e.g., chemical desorption of $H_2O$ is still measurable from the $H_2O$ surface, whereas the strict use of the formula gives zero (Minissale et al. 2016b). Given the much lower efficiencies of RD from water surface observed in experiments, the value of *M* for water surface has been chosen equal to 48 a.m.u. as best matching data from experiments (Minissale et al. 2016b). Recent experiments involving surfaces made of CO and $H_2CO$ ice, showed relatively efficient RD of these two species into the gas (Minissale et al. 2016c), thus advocating quite high effective mass for such surfaces. Any equivalent mass between 80 and 120, indeed agrees with these measurements. Also, in case of CO ice, the binding energy of adsorbates may be lowered with respect to water ice, which also contributes to raising the chemical desorption efficiency on CO ice. Thus, in order not to include any new poorly controlled parameter in the model, we have chosen an effective mass *M* for CO ice equal to 100. Although variations of *M* in the range of 80–120 may change the maximum values of modeled abundances within an order of magnitude, they will not change the general conclusions of this work.

The fraction of kinetic energy retained by the reaction product $\epsilon$ is an important parameter that governs the dependence of the efficiency of RD on surface composition. Its physical meaning is the fraction of kinetic energy retained by a molecule with mass *m* upon collision with a structural element of the surface with mass *M*, under the approximation of classic elastic collisions. As such, the efficiency of RD depends not only on the type of desorbing molecule and enthalpy of reaction, but also on the surface composition, e.g., on the outer layer's composition of a thick icy mantle. In Figure 1, the efficiency of the RD is shown as a function of M for two key species, $H_2CO$ and $CH_3OH$. The vertical text, "CO ice," "water ice," and "bare grain" indicate the *M* value for the corresponding surface types. We assume that the value for "CO ice" is also used for species of similar molar weight, such as $N_2$, $H_2CO$, and $CH_3OH$, since these species have similar molecular masses and no experimental data on scattering of molecules on surfaces consisting of those species are available. These species are expected to constitute a significant fraction of an ice surface under the conditions typical of prestellar cores. Therefore, the total efficiency of RD is calculated as a sum of efficiencies of RD on different types of surfaces: bare grain, water ice, "heavy ice" (CO + $N_2$ + $H_2CO$ + $CH_3OH$ ices) times the fraction of the corresponding surface type within the whole surface.

### 2.4. Updates to the Chemical Network

Since Vasyunin & Herbst (2013b), several important studies concerning chemistry of COMs in cold environments were published. We updated our chemical network with new gas-phase reactions proposed in Shannon et al. (2013, 2014) and Balucani et al. (2015). Namely, Shannon et al. (2013, 2014) discovered that reactions between hydroxyl radical OH and oxygenated hydrocarbons such as methanol and dimethyl ether are efficient at low temperatures due to tunneling through activation barrier and formation of a hydrogen-bonded complex:

$$OH + CH_3OH \rightarrow CH_3O + H_2O \quad (8)$$

$$OH + CH_3OCH_3 \rightarrow CH_3OCH_2 + H_2O. \quad (9)$$

Also, Balucani et al. (2015) proposed a gas-phase chemical link between dimethyl ether ($CH_3OCH_3$) and methyl formate ($HCOOCH_3$) through the radical $CH_3OCH_2$:

$$(F, Cl) + CH_3OCH_3 \rightarrow CH_3OCH_2 + (HF, HCl) \quad (10)$$

$$CH_3OCH_2 + O \rightarrow HCOOCH_3 + H. \quad (11)$$

The discovery of a new class of gas-phase reactions with hydroxyl radical efficient at low temperatures as well as a chemical link between dimethyl ether and formaldehyde are important findings for the problem of formation of COMs. To the best of our knowledge, this combination of new reactions has not been included in a full-scale astrochemical model before.

The gas-phase formation route of formamide ($NH_2CHO$) has been updated according to the recent studies by Barone et al. (2015) and Skouteris et al. (2017). Using quantum chemical calculations, Skouteris et al. (2017) updated the previous result by Barone et al. (2015), and estimated the rate constants for the reaction

$$NH_2 + H_2CO \rightarrow NH_2CHO + H \quad (12)$$

to be equal to $\alpha = 7.8 \times 10^{-16}$ cm$^3$ s$^{-1}$, $\beta = -2.56$, $\gamma = 4.88$ K. This gives the value of modified Arrhenius rate constant, which is defined as $k = \alpha \cdot (T/300\,\mathrm{K})^{\beta} \cdot \exp(-\gamma/T)$ equal to $2.9 \times 10^{-11}$ cm$^3$ s$^{-1}$ at 10 K. As such, reaction (12) is expected to be a major route of formation of formamide in cold clouds (as long as $NH_2$ and $H_2CO$ are abundant in the gas phase).

Finally, we altered the gas-phase chemistry of acetaldehyde ($CH_3CHO$) by including four gas-phase reactions in our model:

$$CH + CH_3OH \rightarrow CH_3CHO + H, \quad (13)$$

$$CH + CH_3OH \rightarrow CH_3 + H_2CO, \quad (14)$$

$$C + CH_3CHO \rightarrow C_2H_4 + CO \quad (15)$$

and

$$CH_3 + HCO \rightarrow CH_3CHO + h\nu. \quad (16)$$

Processes (13) and (14) are the two most likely outcomes of the reaction between CH and $CH_3OH$ experimentally studied by Johnson et al. (2000). They found this reaction to be barrierless, pressure-independent with negative dependence on temperature.

**Table 1**
Important Reactions Governing Chemistry of Complex Organic Molecules in Cold Environments

| Reaction | Rate at 10 K, $cm^3\ s^{-1}$ | Reference |
|---|---|---|
| $OH + CH_3OH \rightarrow CH_3O + H_2O$ | 1.1(−10) | S13, A16 |
| $OH + CH_3OCH_3 \rightarrow CH_3OCH_2 + H_2O$ | 1.7(−11) | S14 |
| $F + CH_3OCH_3 \rightarrow CH_3OCH_2 + HF$ | 2.0(−10) | HN96 |
| $Cl + CH_3OCH_3 \rightarrow CH_3OCH_2 + HCl$ | 2.0(−10) | W88 |
| $CH_3OCH_2 + O \rightarrow HCOOCH_3 + H$ | 2.0(−10) | HN96, S05 |
| $CH_3O + CH_3 \rightarrow CH_3OCH_3 + h\nu$ | 3.0(−10) | VH13, B15a |
| $CH + CH_3OH \rightarrow CH_3CHO + H$ | 1.8(−8) | J00 |
| $CH + CH_3OH \rightarrow CH_3 + H_2CO$ | 1.6(−7) | J00 |
| $C + CH_3CHO \rightarrow C_2H_4 + CO$ | 5.4(−10) | HI99 |
| $C + H_2CO \rightarrow CO + CH_2$ | 6.2(−10) | HI99 |
| $CH_3 + HCO \rightarrow CH_3CHO + h\nu$ | 5.0(−11) | NIST |
| $NH_2 + H_2CO \rightarrow NH_2CHO + H$ | 2.9(−11) | S17 |

**Note.** a(-b) stands for $a \times 10^{-b}$. $\alpha$, $\beta$, and $\gamma$ are the coefficients in the modified Arrhenius expression for the reaction rate coefficient: $k = \alpha \cdot (T/300)^{\beta} \cdot \exp(-\gamma/T)$. S13 refers to Shannon et al. (2013), A16 refers to Antinolo et al. (2016), S14 refers to Shannon et al. (2014), HN96 refers to Hoyermann & Nacke (1996), W88 refers to Wallington et al. (1988), S05 refers to Song et al. (2005), VH13 refers to Vasyunin & Herbst (2013b), B15a refers to Balucani et al. (2015), S17 refers to Skouteris et al. (2017), J00 refers to Johnson et al. (2000), HI99 refers to Husain & Ioannou (1999). URL for NIST Chemical Kinetics Database: http://kinetics.nist.gov/kinetics/index.jsp.

The total rate of the reaction between CH and $CH_3OH$ at 300 K is reported by Johnson et al. (2000) to be $2.5 \times 10^{-10}$ $cm^3\ s^{-1}$ with a temperature-dependent Arrhenius factor −1.93. Since channel (14) is more thermodynamically favorable than channel (13), we assume 90% probability for the channel (14) to occur versus 10% probability for the channel (13) (see Table 1). Interestingly, channel (13) is added to the UDFA12 database (McElroy et al. 2013), but is absent in the KIDA database (Wakelam et al. 2015). On the contrary, channel (14) does not exist in UDFA12, but is added to KIDA.

Reaction (15) is taken from Husain & Ioannou (1999). This reaction is expected to reduce the gas-phase abundance of acetaldehyde at early times when atomic carbon is relatively abundant in the gas phase. A similar reaction between carbon atoms and formaldehyde from Husain & Ioannou (1999) is also added to the chemical network to better constrain the abundance of $H_2CO$ at early times.

The rate for reaction (16) has been taken from Callear & Cooper (1990), who studied the reaction experimentally, under the temperature range of 373–473 K. We assume that the rate of reaction (16) remains the same down to 10 K: $5 \times 10^{-11}$ $cm^3\ s^{-1}$; though, it is possible that at low temperature the rate of the reactions could be higher due to more efficient stabilization of initially vibrationally excited $CH_3CHO$. The details of all newly included reactions are summarized in Table 1.

### 2.5. Physical Model of L1544 and Initial Conditions for Chemistry

To model the radial profiles of COMs in L1544, we use the results from a 1D physical model of the prestellar core developed by Keto & Caselli (2010), see Figure 2. In the core, one can single out the very dense and dark central part, an intermediate shell with moderate density, and the outer part

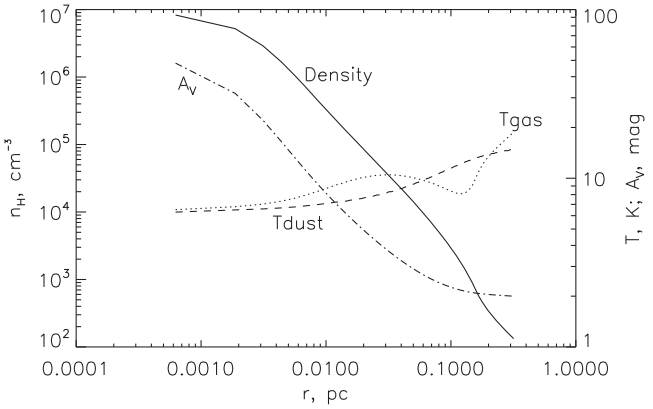


**Figure 2.** Physical structure of L1544 from Keto & Caselli (2010). Note that gas and dust temperature slightly decrease from the edge to center from ≈20 K to ≈7 K, while the visual extinction rises sharply from 2 mag to more than 50 mag.

with low density and penetrating UV field. We took the visual extinction at the edge of the core equal to $A_V = 2$ mag to simulate the fact that L1544 is embedded in a molecular cloud. In total, our physical model has 128 radial points with different physical conditions. For each point, chemistry has been calculated independently using our 0D chemical model. Single grain size of $10^{-5}$ cm is used to calculate visual extinction and chemical evolution in the current study.

To obtain the initial abundances of the molecular species at $t = 0$ yr in our simulations, we ran the chemical code for the time span of $10^6$ years using physical conditions typical for a translucent cloud: hydrogen column density $n_H = 10^2$ $cm^{-3}$, temperature $T = 20$ K, visual extinction $A_V = 2$ mag, and "low metals" atomic initial conditions, corresponding to the values listed as EA1 in Table 1 in Wakelam & Herbst (2008). Final abundances from these simulations were taken as initial values for the simulations presented in this study.

The mobility of species on grain surfaces is a matter of debate in the astrochemical community. At low temperatures typical for prestellar clouds, only a limited number of species should be mobile on grain surfaces. Among them, atomic and molecular hydrogen. For these species, the main source of mobility is assumed to be quantum tunneling through a rectangular barrier of width 1 Å separating the binding sites (e.g., Hasegawa et al. 1992). Although the efficiency of quantum tunneling for H and $H_2$ on grain surfaces has been debated for a long time, no solid agreement is reached on this point so far (see, e.g., for review, Hama & Watanabe 2013). In this study, we enabled tunneling for diffusion of H and $H_2$ in the model. The importance of tunneling for the simulations results is highlighted in Section 4. Tunneling was also claimed to be efficient for oxygen atoms at low temperatures (Minissale et al. 2013). However, in a more recent experiment by He et al. (2014), mobility of atomic oxygen was only observed at $T \sim 40$ K, which contradicts the assumption of efficient tunneling for O atoms. As such, we have chosen not to include atomic oxygen tunneling in our model. For other species, the main diffusion mechanism is due to thermal hopping, with a rate defined by the binding–desorption energy ratio, $E_b/E_D$. Following recent estimates by Minissale et al. (2016a), we select the value of $E_b/E_D = 0.55$. However, at dust temperatures ∼10 K with enabled tunneling for H and $H_2$ diffusion, this value is not expected to play a crucial role for the chemical evolution of icy mantles, even when set to the lowest value considered in the

literature, $E_b/E_D = 0.3$ (Hasegawa et al. 1992). As mentioned above, for bulk chemistry, this value is doubled. However, at low dust temperatures, bulk chemistry is well separated from surface chemistry, and all the essential processes affecting abundances of gas-phase species discussed below are impacted by the composition of the surface layers of icy mantles. This is explicitly simulated in the model in a framework of a three-phase formalism "gas-surface-bulk."

Tunneling through potential barriers is not only important for surface mobility of light species such as H and $H_2$, but also for calculations of the rates of reactions with activation barriers. Several approaches have been proposed to calculate the transmission probabilities through the reaction activation barriers on the surface. Hasegawa et al. (1992) proposed to calculate the transmission probability through the rectangular activation barrier of 1 Å width, while Garrod & Pauly (2011) proposed to use the width of the rectangular activation barrier of 2 Å. Also, Taquet et al. (2013), recently employed the Eckart's model to calculate the transmission probability. Here, we use transmission probabilities through rectangular barriers with widths of $a = 1.2$ Å. Our simulations show that the composition of the gas phase in the considered model is stable with respect to the choice of the width $a$ in the range of [1.0–1.5] Å, while the composition of the bulk of the ice is quite sensitive to the exact value of $a$, and resembles the observed ice composition best at $a = 1.2$ Å. As such, by the choice of the particular value of $a$ we do not aim to put exact constraints on transmission probabilities for reactions with activation barriers in interstellar ice. Instead, we aim to show that our model is capable of reproducing abundances of COMs in L1544, and produce a reasonable composition of the icy mantles of interstellar grains simultaneously.

## 3. Results

### 3.1. Radial Profiles of Chemical Abundances

Observed values of fractional abundances of species toward prestellar cores and other astronomical objects are usually inferred from the observed column densities of species divided by the column density of $H_2$. This provides abundances averaged over the line of sight. As such, in compact objects with strong gradients of physical parameters such as prestellar cores, the abundances derived from column densities differ from true local fractional abundances. However, since the goal of this work is to investigate the chemistry of COMs in different parts of L1544, below in most cases we present modeled true local fractional abundances of species calculated as volume concentration of a species divided by volume concentration of $H_2$ versus time and radius. When presented, column densities are calculated following the expressions (1) and (2) in Section 7 in Jiménez-Serra et al. (2016).

Since abundances of species evolve with time in each point of L1544, it is important to determine the time that gives best agreement with observations. Our model does not include any treatment of dynamical evolution of L1544, neither treatment of collapse nor mixing between gas parcels. Also, the "chemical age" of an astrophysical object does not necessarily correspond to its physical age. Therefore, we have chosen the depletion factor of CO toward the center of L1544 as an estimation of the time for which the comparison of modeled chemistry with observations should be performed. The depletion factor of CO, defined as the ratio between the reference and observed CO column densities, was measured by Caselli et al. (1999) as ∼10 toward the dust peak position, the center of our spherically symmetric core model. This depletion factor of CO can be easily calculated as a function of time in our model. Figure 3 shows that the CO depletion factor becomes similar to the observed one after a time of $\sim 10^5$ years. Therefore, we present modeled radial abundances of species in L1544 for this time, unless otherwise stated.

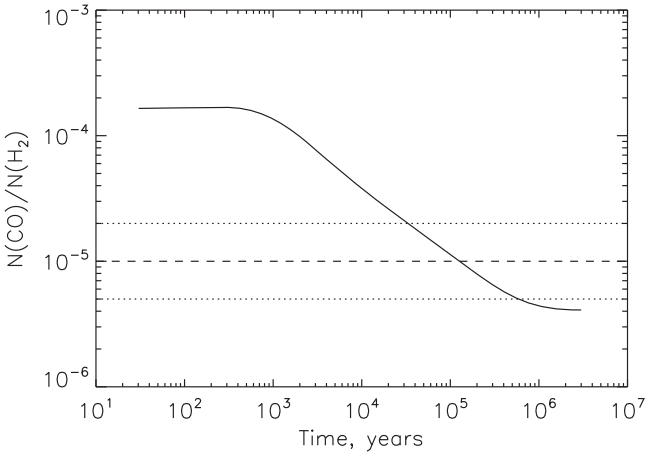


**Figure 3.** CO-to-$H_2$ column density ratio. The value observed toward the center of L1544 is reached within $10^5$ years, with our assumption of a static cloud. The observed value according to Caselli et al. (1999) is plotted with the dashed horizontal line. The factor of two uncertainty in the observed value is shown with the dotted horizontal lines.

In Figure 4, the top panel, radial profiles of selected simple species typically observed toward cold dark clouds are shown. By $10^5$ years, all simple molecules except CO exhibit hump-like profiles. toward the center of L1544, species are significantly depleted due to high density and low temperature. In the outer parts of the cloud, at radial distances $R \geqslant 0.03$ pc, the visual extinction drops below 3 mag, thus making most molecules vulnerable to photodissociation by the interstellar UV field. $H_2$ and CO are the exceptions, because of the effect of self-shielding and shielding by dust. The gas-phase abundance of CO drops sharply at $R \leqslant 0.03$ pc, where the gas density is higher than $10^5$ cm$^{-3}$, in agreement with findings by Caselli et al. (1999). Abundance profiles of two key nitrogen-bearing species in prestellar clouds, $NH_3$ and $N_2H^+$, exhibit great similarity, with ammonia being about two orders of magnitude more abundant. This behavior is typical of low-mass dense cores, including L1544, as found by Tafalla et al. (2002). Radial behavior of $HCO^+$ is similar to the best-fit Model 3 in Caselli et al. (2002). $N_2H^+$ and $HCO^+$ are the two most abundant positive ions, thus reflecting the ionization degree. In turn, it appears similar to the measurements of Caselli et al. (2002). In the bottom panel of Figure 4, radial profiles of column density ratios of simple species wrt. column density of $H_2$ convolved with a telescope beam size of 26″ are shown: $N(X)/N(H_2)$. This corresponds to the abundances of species directly inferred from observations by Jiménez-Serra et al. (2016). One can see that column density profiles show flatter profiles than local fractional abundances of species. Indeed, the CO-to-$H_2$ column density ratio decreases by an order of magnitude toward the outer part of the core, instead of six orders of magnitude for local volume abundances. For $NH_3$, the $N(NH_3)/N(H_2)$ ratio decreases by an order of magnitude instead of two and a half orders for local volume abundances.

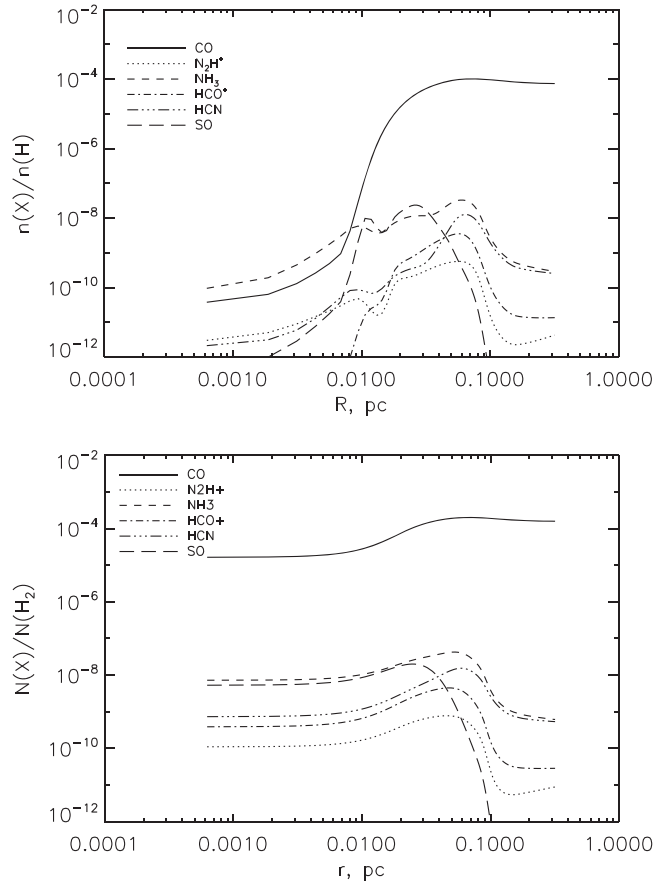


**Figure 4.** Radial profiles of abundances (top panel) and convolved with a telescope beam size of 26″ column densities (bottom panel) of simple species after $10^5$ years of chemical evolution in L1544.

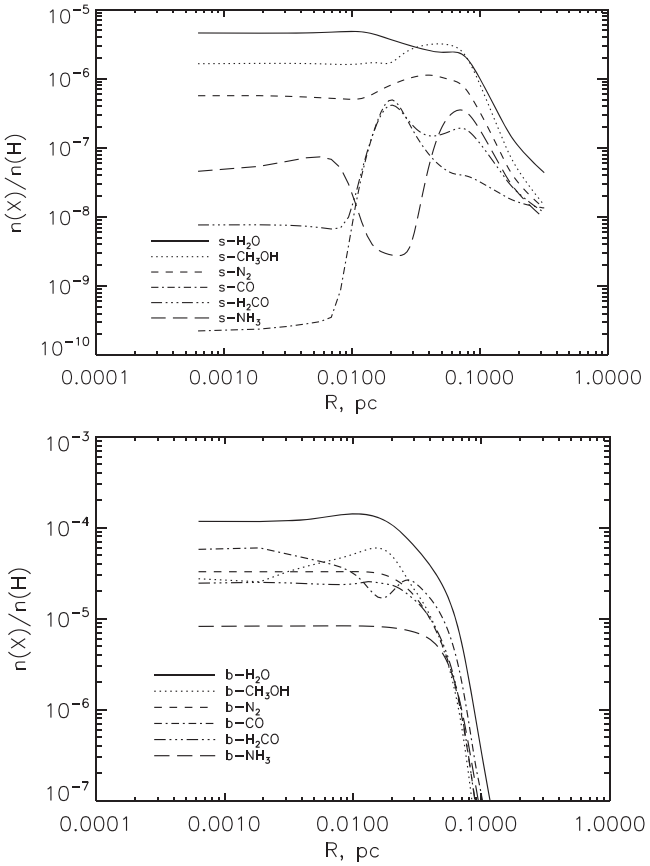


**Figure 5.** Composition of the surface ice layers (top) and bulk ice (bottom) at L1544 vs. radius at $1.6 \times 10^5$ years.

Such even behavior of column density ratios match observational data on molecular distributions in L1544 better than local volume abundances, especially for $NH_3$, for which observations are consistent with $N(NH_3)/N(H_2)$ increasing toward the center of the core (Tafalla et al. 2004), while the $N(N_2H^+)/N(H_2)$ column density ratio appears to be constant. This "extra" depletion of N-bearing species compared to observations may be due to the fact that dynamics is ignored in our simulations (see Section 4 for further discussion). Such behavior for N-bearing molecules was also present in our previous chemical models. Therefore, updates to our model concerning efficient RD and new gas-phase chemistry of COMs does not affect noticeably well-established chemistry of simple species in the gas phase, and we do not discuss it further.

Let us now consider the chemistry in icy mantles of interstellar grains. Advanced treatment of icy mantles utilized in this study, allows us to consider the chemical evolution of ice surface and bulk ice separately. Since mobility of species on the surface and inside the bulk is different, and desorption is only possible from the surface, bulk and surface usually have different chemical compositions. In Figure 5, the composition of ice surface (top panel) and bulk ice (bottom panel) is shown vs. radius after $10^5$ years of evolution. Plotted species are the most abundant ones on the surface and in the bulk ice, respectively, at a radial distance of $R = 0.02$ pc.

The "surface" of icy mantles in our model consists of a number of molecules corresponding to four monolayers of ice. We prefer not to distinguish individual monolayers in the ice, because bulk diffusion of species is enabled in the model. Under this assumption, individual monolayers cannot be unambiguously identified. Besides the new treatment of RD, we did not introduce any new chemical processes in our model. Therefore, the chemical evolution on the ice surface is, in general, similar to that described in previous studies (Garrod & Pauly 2011; Vasyunin & Herbst 2013a).

In the entire range of distances from the center of the cloud, the chemical composition of ice surface does not differ significantly. Since, in our model, we enable quantum tunneling for H and $H_2$ and diffusion/desorption energy ratio $E_b/E_D = 0.55$, the major constituents of the ice surface are water, methanol, molecular nitrogen, as well as somewhat less abundant carbon monoxide, formaldehyde, and ammonia. While CO and $N_2$ are mainly accreted from the gas phase, other major species are formed on the surface in hydrogenation reactions. Water is mainly formed in surface reaction between atomic hydrogen and hydroxyl radical, but it is also accreted from the gas phase, though to less extent. Methanol and formaldehyde are formed during the hydrogenation of the CO molecule as described in Section 2.2. Quantum tunneling for diffusion and passing through activation barriers of reactions with H and $H_2$ makes CO hydrogenation efficient, thus leading to the abundance of $CH_3OH$ on the surface higher than abundances of CO and $H_2CO$. Note that, if tunneling for diffusion or passing through reaction activation barriers is neglected, our model cannot produce methanol in the ice in appreciable amounts. Interestingly, at timescales after $10^5$ years, methanol and water on the surface become

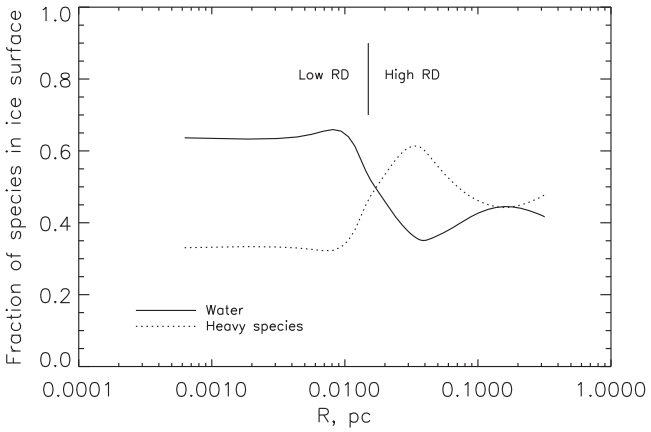


**Figure 6.** Fraction of water and "heavy species" in the surface layers of icy mantles of grains vs. radius after $10^5$ years of evolution. Reactive desorption is only efficient from the fraction of surface consisting of "heavy species."

chemically related, because a significant fraction of atomic hydrogen and hydroxyl radical on the surface at that time is produced by the photodissociation of methanol by cosmic-ray-induced photons in the center of the core, or by interstellar UV photons at the edge of the cloud. The fraction of surface covered with "heavy" species (mainly methanol) vary from ∼0.35 at $R \leqslant 0.01$ pc to ∼0.65 at outer radii (Figure 6). This shift of balance between water and heavy species is mostly due to slightly different rates of photodissociation of water and methanol. In our model, the exponential factor for photorates $\gamma_{CH_3OH} = 2.3$, while $\gamma_{H_2O} = 2.2$ (van Dishoeck et al. 2006), which makes water start to photodissociate at somewhat smaller radii with higher visual extinction than methanol.

Although the composition of the bulk of ice does not directly affect the abundances of gas-phase COMs in our model, it is important to make sure that adopted parameters of our model do not lead to bulk composition that contradicts the observational data. The composition of the bulk of the ice at $1.6 \times 10^5$ years is presented in Figure 5, bottom panel. In bulk ice, solid water is the dominant species. Solid carbon monoxide is the second most abundant bulk ice constituent in the inner and outer regions of L1544 ($R \leqslant 0.007$ pc, $R \geqslant 0.03$ pc) with an abundance of ∼50% that of solid water. In the intermediate part of the cloud (0.007 pc $\leqslant R \leqslant$ 0.03 pc) the abundance of CO is reduced, and the second most abundant species in the bulk ice is methanol with a maximum fraction of ∼45% with respect to solid water. Averaged over the whole L1544, abundances of CO and $CH_3OH$ in the bulk of ice with respect to solid water are ∼35% and ∼28%, respectively. Note that the bulk abundance of methanol with respect to solid water is reduced in contrast to its surface value because the methanol that was buried in the bulk after its formation on the surface is partly dissociated via cosmic rays. While the abundance of solid $N_2$ is not inferred from observations due to the low strength of the fundamental N–N stretch band of $N_2$ in ices (Sandford et al. 2001), abundances of solid CO and $CH_3OH$ have been estimated observationally. Öberg et al. (2010) provided average observational fractions of CO and $CH_3OH$ in low-mass clouds to be 29% and 3%, respectively, which somewhat differs from our modeling results. On the other hand, the fraction of methanol in the ice vary by approximately an order of magnitude among different clouds, reaching 25% wrt. solid water in some cases, e.g., Class 0 protostars (Pontoppidan et al. 2004), which are close

**Table 2**
Composition of Icy Mantles Averaged Over the Whole L1544 in Main Model (MM)

| Species | Abundance wrt. solid water, % |
|---|---|
| $H_2O$ | 100 |
| CO | 35 |
| $CH_3OH$ | 28 |
| $N_2$ | 26 |
| $H_2CO$ | 19 |
| $NH_3$ | 7 |
| $CH_4$ | 6 |
| $H_2O_2$ | 4 |

**Note.** Ice constituents with abundances larger than 1% wrt. solid water are shown.

evolutionarily to the prestellar cores such as L1544. As such, we believe that the $CH_3OH/CO$ ratio obtained in the ice by our model does not represent a major issue in this study. The abundance of ammonia in the ice is ∼7% wrt. water, which is similar to observed values. Solid carbon dioxide $CO_2$ is one of the main constituents of the ice according to observations (e.g., Öberg et al. 2010). However, in our simulations, it is missing because it is likely formed at the onset of a cold dense cloud formation from a warmer translucent cloud at $T_{dust} \sim 20$ K (Mennella et al. 2006; Garrod & Pauly 2011; Vasyunin & Herbst 2013a). Since in our simulations we do not follow the cloud formation with time-dependent physical conditions, we miss this phase. Note, however, that protonated carbon dioxide, $HOCO^+$, has recently been observed in L1544 (Vastel et al. 2016), which implies the presence of gas-phase $CO_2$, too. Nevertheless in the model discussed in this study, neither gas-phase nor solid $CO_2$ and its protonated form do not affect the chemistry of COMs. Abundances of major ice constituents in the whole core are summarized in the Table 2.

### 3.2. Chemistry at the COMs Peak

Modeled abundances of complex organic species in L1544 exhibit both significant temporal (Figure 7, bottom panel) and radial (Figure 8, bottom panel) variations, as well as the abundances of chemically related precursor species (the same figures, upper panels). The peak abundances of COMs are reached within $10^5$–$2 \times 10^5$ years of chemical evolution, which corresponds to the time when the observed depletion factor of CO is attained in our model (Figure 3). This time is higher than the time estimated by Caselli et al. (1999; $10^4$ years), using CO depletion factor and freeze-out rate. However, taking into account the uncertainty by a factor of two in the depletion factor claimed by Caselli et al. (1999), and possibly smaller depletion rate due to non-thermal evaporation of species, which was not considered by Caselli et al. (1999), we believe that our results do not contradict observational constraints.

Maximum abundances of most COMs including $HCOOCH_3$, $CH_3OCH_3$, and $NH_2CHO$ are reached for distances between ∼0.01–0.02 pc from the center of L1544, that roughly corresponds to the position of a ring-like emission of methanol observed by Bizzocchi et al. (2014) and of COMs deduced by Vastel et al. (2014). As shown by Jiménez-Serra et al. (2016), COMs are indeed enhanced in an outer shell centered at a distance of 0.02 pc (equivalent to 4000 au) with respect to the

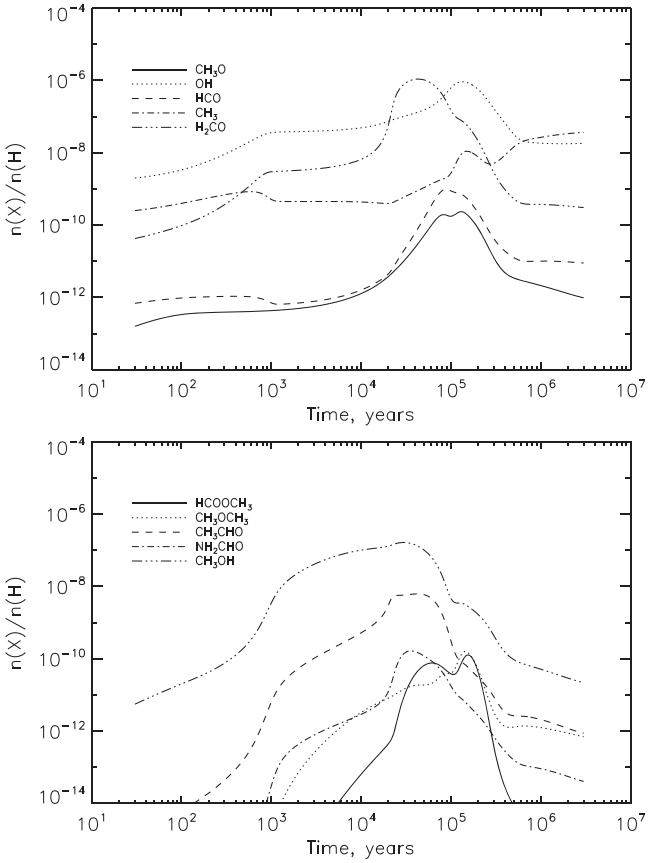


**Figure 7.** Temporal evolution of the abundances of COMs and related species at the distance of 0.015 pc from the center of L1544. This location is chosen as representative for the chemistry at the COMs peak.

center of the core. Peak abundances of methyl formate, dimethyl ether, and formamide reach approximately (3–4) $\times$ $10^{-10}$ wrt. total hydrogen nuclei. The comparison between models and observations versus time and radial distance in L1544 is shown in Figure 9. In the left and middle columns, an agreement for illustrative models is shown (see below). In the right column, the agreement for the Main model (MM) under discussion is presented. The agreement was calculated using the following expression:

$$F(r,t) = \sum_{i=1}^{N_{\rm species}} \left( \frac{X^i_{\rm obs} - X^i_{\rm mod}(r,t)}{X^i_{\rm obs} + X^i_{\rm mod}(r,t)} \right)^2, \quad (17)$$

where $X_{\rm mod,obs}$ are the modeled and observed column densities of species. Modeled column densities are smoothed over the Gaussian beam of 26″ size in order to simulate the observed abundances and column densities taken from Jiménez-Serra et al. (2016) toward the position of the "methanol peak."[5] ($r$, $t$) is the location in the phase space (radius, time). The species used to calculate the agreement are $HCOOCH_3$, $CH_3OCH_3$, $NH_2CHO$, $CH_3CHO$, $CH_3O$, and $CH_3OH$. As such, an agreement map shows at which time(s) and for which radii the modeled column densities fit the observational data at the "methanol peak" in L1544, located at ~0.02 pc or ~4000 au from the center of L1544.

[5] This position corresponds to the peak of the $CH_3OH$ emission reported by Bizzocchi et al. (2014), which is ~4000 au (0.019 pc) away from the dust emission peak (see also Jiménez-Serra et al. 2016 for more details).

In Table 3, the best-fit modeled column density ratios of species wrt. $H_2$–$N(X)/N(H_2)$, corresponding to the abundances inferred from observations for L1544—are shown, as well as the observed abundances obtained by Jiménez-Serra et al. (2016). Also, for comparison, abundances of COMs in L1689B and B1-b are shown, taken from Bacmann et al. (2012) and Cernicharo et al. (2012). These two sources have gas and dust temperatures similar to those in L1544. Also, column densities of COMs observed toward these cores are of the same order of magnitude as in L1544 (~$10^{12}$ $cm^{-2}$) suggesting similar extinctions in the regions of COMs formation, thus making reasonable comparison with model predictions originally made for L1544. The minimal value of $F(r, t)$ is reached at 1.6 $\times$ $10^5$ years and at the radius of 0.015 pc. This time is similar to that at which the model also reproduces the CO column density (see Figure 3). This indicates that chemistry of COMs clearly belongs to a so-called early chemistry type. Also, the spatial location of the best-fit position is roughly similar to the location of the "methanol peak" in L1544. Since the values in Table 3 have been calculated by averaging the predicted column densities within a beam of 26″ (this is the beam size in the observations by Jiménez-Serra et al. 2016), they are somewhat different from true local fractional abundances of species obtained with the chemical model and discussed below.

Let us now focus on the chemistry of COMs in our model near the location of best-fit abundances of COMs, namely at radial distance 0.015 pc. In general, the formation of all complex organic species considered in this study follows the scenario proposed in Vasyunin & Herbst (2013b). In that scenario, COMs in the cold gas are formed mainly via gas-phase reactions from precursor species that are formed on grains (totally, or at least in a significant part) and then ejected into the gas phase via efficient RD. While in Vasyunin & Herbst (2013b), the majority of gas-phase reactions important for the formation of COMs are ion-molecule reactions, in this study, new gas phase neutral–neutral reactions play an important role too.

Dimethyl ether ($CH_3OCH_3$) and methyl formate ($HCOOCH_3$) exhibit very similar radial (see Figure 8) and temporal (see Figure 7) behavior. Dimethyl ether is produced via the reaction

$$CH_3 + CH_3O \rightarrow CH_3OCH_3 + h\nu, \quad (18)$$

proposed by Vasyunin & Herbst (2013b). Following the comment by Balucani et al. (2015) on the rate of this reaction, we updated the value of the rate coefficient to 3.0 $\times$ $10^{-10}$ $cm^3$ $s^{-1}$ (see Table 1). $CH_3$ is formed as a product of dissociative recombination of $CH_5^+$. This formation route in the Main model (MM) is assisted by a gas-phase reaction

$$CH_3O + H \rightarrow CH_3 + OH, \quad (19)$$

also introduced in Vasyunin & Herbst (2013b), and leads to the increase of the abundance of $CH_3$ by a factor of three with respect to pure ion-molecule formation. About 55% of the methoxy radical $CH_3O$ in the gas phase is produced via the gas-phase reaction

$$OH + CH_3OH \rightarrow CH_3O + H_2O, \quad (20)$$

while another 45% of $CH_3O$ is ejected to the gas via RD after the surface production in the reaction

$$s - H + s - H_2CO \rightarrow s - CH_3O. \quad (21)$$

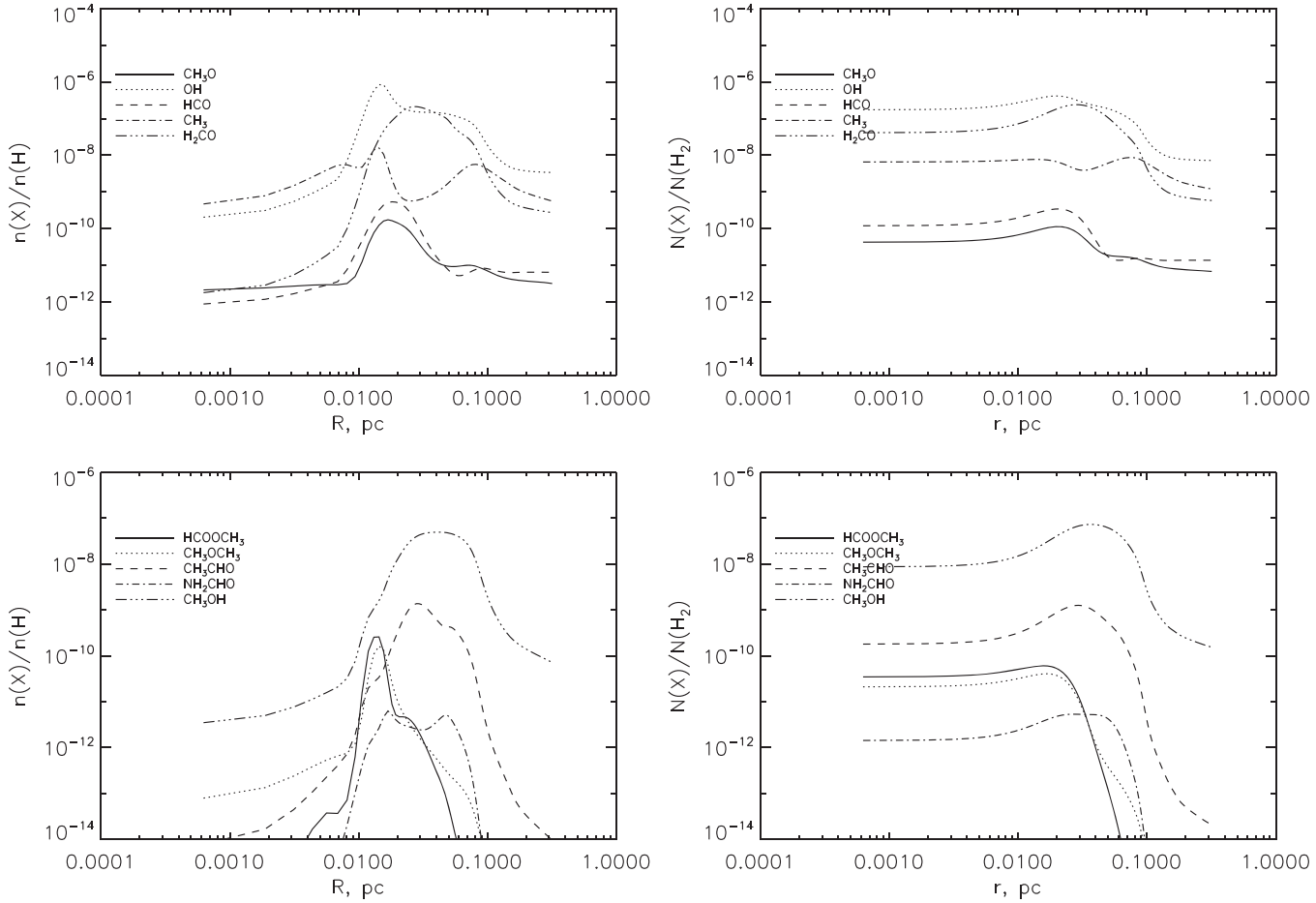


**Figure 8.** Radial profiles of abundances of COMs and some related species at $1.6 \times 10^5$ years (left column) and simulated radial profiles of abundances as obtained as column density ratios observed with the 26″ telescope beam (right column). $1.6 \times 10^5$ years is the time of the best agreement (minimal $F(r, t)$, see the text) between the modeled and observed abundances of species inferred from column densities. All species clearly exhibit peaks at radial distances between 0.01 pc and 0.03 pc, which matches the ring-like distribution of $CH_3OH$ observed in L1544 (Bizzocchi et al. 2014).

Shannon et al. (2013) found reaction (20) to exhibit strong negative dependence on temperature due to the formation of a hydrogen-bonded complex that lives sufficiently long to undergo quantum mechanical tunneling through the activation barrier of the reaction and to form products. Antinolo et al. (2016) confirmed this result, and measured the temperature-dependent rate of the reaction in the range of 22–64 K. Extrapolation to 10 K gives the rate of the reaction equal to $1.1 \times 10^{-10}$ cm$^3$ s$^{-1}$, which is three times faster than the rate adopted for this reaction in Vasyunin & Herbst (2013b). Thus in this work, the methoxy radical reaches the fractional abundance of $2.5 \times 10^{-10}$ wrt. H (see Figure 8, upper panel), which is higher than in the model by Vasyunin & Herbst (2013b) and about an order of magnitude higher than observed by Bacmann & Faure (2016) for several prestellar cores other than L1544, and by factors of ∼5–10 in L1544 (Jiménez-Serra et al. 2016). Note, however, that the $CH_3O$ abundance in our model is mainly controlled by the pair of reactions (18) and (20). Rates of both reactions are poorly known. Thus, in principle, by varying these reaction rates, one can modify the abundance of $CH_3O$ widely, almost without changing the abundance of $CH_3OCH_3$. More theoretical and/or laboratory work needs to be carried out to put more stringent constraints on chemical models.

Methyl formate ($HCOOCH_3$) has two main production channels. Approximately two-thirds of the total methyl formate production belongs to the reaction

$$O + CH_3OCH_2 \rightarrow HCOOCH_3 + H. \quad (22)$$

This reaction has been studied by Hoyermann & Nacke (1996) and Song et al. (2005), and introduced into astrochemical models by Balucani et al. (2015). The fractional abundance of atomic oxygen in our model after $10^5$ years is $6 \times 10^{-8}$ wrt. H. The second reactant, $CH_3OCH_2$, is mainly produced via the reactions

$$CH_3OCH_3 + OH \rightarrow CH_3OCH_2 + H_2O. \quad (23)$$

This reaction has been studied in Shannon et al. (2014), who showed that it is efficient at low temperatures due to a similar mechanism as that for reaction (20). This is in contrast to Balucani et al. (2015), who pointed out the existence of a chemical link between $CH_3OCH_3$ and $HCOOCH_3$ via the reaction (22), but claimed the main formation routes of $CH_3OCH_2$ to be reactions between dimethyl ether and elemental fluorine (F) and chlorine (Cl). In our model, both chemical elements are highly depleted in the gas phase, having fractional abundances of $2.3 \times 10^{-17}$ and $6.3 \times 10^{-11}$ wrt. H, respectively, at the time of $10^5$ years. Therefore, the formation

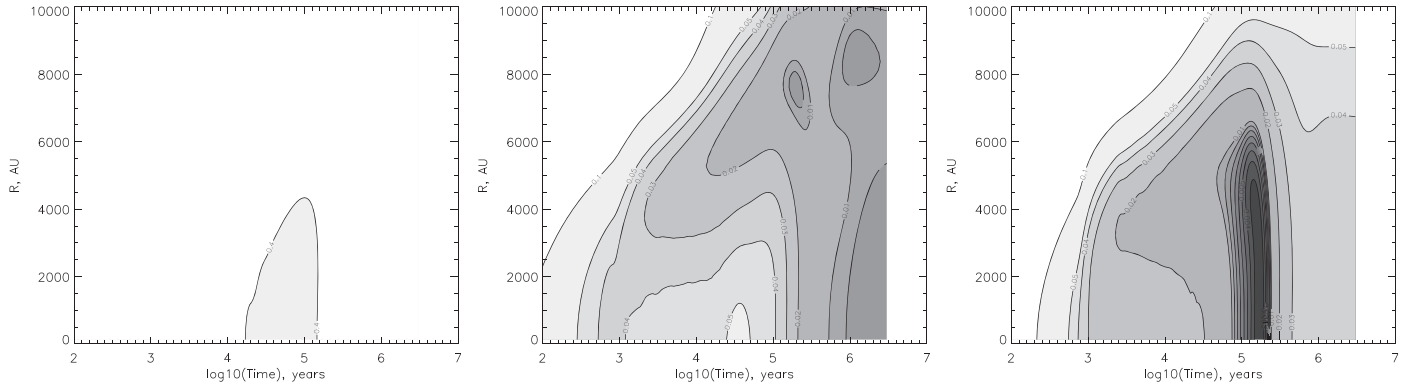


**Figure 9.** Agreement maps for column densities of COMs for the model with no reactive desorption (left column), model with single 10% efficiency of reactive desorption (middle column), and model with advanced treatment of reactive desorption (right column). Modeled column densities used for comparison are smoothed over the 26″ Gaussian beam. Darker filling indicates the better agreement between model and observations. Only the model with advanced treatment of reactive desorption exhibit agreement with observations for both abundances and column densities of COMs at the time corresponding to the observed amount of CO freeze-out, and radial location similar to the observed location of the "methanol peak."

**Table 3**
Observed and Best-fit Modeled Fractional Abundances of Organic Species Detected in Cold Interstellar Clouds, Obtained As Ratios of Column Densities $N(X)/N(H_2)$

| Species | Main model (MM) | Observations | | |
|---|---|---|---|---|
| | | L1544 | L1689b | B1-b |
| $HCOOCH_3$ | 6.0(−11) | 1.5(−10) J | 7.4(−10) B | 2.0(−11) C |
| $CH_3OCH_3$ | 4.0(−11) | 5.1(−11) J | 1.3(−10) B | 2.0(−11) C |
| $NH_2CHO$ | 3.8(−12) | ⩽8.7(−13) J | … | … |
| $CH_3CHO$ | 5.8(−10) | 2.1(−10) J | 1.7(−10) B | 1.0(−11) C |
| $CH_3O$ | 1.0(−10) | 2.7(−11) J | 3.3(−11) BF | 4.7(−12) C |
| HCO | 4.6(−10) | … | 3.6(−10) BF | … |
| $H_2CO$ | 4.8(−08) | … | 1.3(−09) B | 4.0(−10) M |
| $CH_3OH$ | 2.7(−08) | 6.0(−9) V | … | 3.1(−09) O |

**Note.** a(-b) stands for $a \times 10^{-b}$. B refers to Bacmann et al. (2012), BF refers to Bacmann & Faure (2016; the fractional abundances derived as fraction of column densities provided in Tables 6 and 7 of BF divided by the $H_2$ column density value of $3.6 \times 10^{22}$ cm$^{-2}$ taken from Bacmann et al. 2016), C refers to Cernicharo et al. (2012), J refers to the abundances of COMs measured toward the position of the "methanol peak" defined by Jiménez-Serra et al. (2016), M refers to Marcelino et al. (2005), O refers to Öberg et al. (2010), and V refers to Vastel et al. (2014). Values for Main model (MM) are smoothed for a telescope beam size of 26″ to allow comparison with observed values by Jiménez-Serra et al. (2016).

of $CH_3OCH_2$ in our model is dominated by reaction (23) instead of by reactions between dimethyl ether and F or Cl.

From this analysis, the hydroxyl radical (OH) appears to be the key chemical species for the chemistry of methyl formate and dimethyl ether in the cold gas. The fractional abundance of OH reaches the value of $\sim 7 \times 10^{-7}$ after $10^5$ years of evolution and at radial distance $R = 0.015$ pc. This is somewhat higher than the OH abundance estimated by Harju et al. (2000) who found it to be about $1 \times 10^{-7}$ wrt. H. However, taking into account the intrinsic uncertainties in astrochemical models (Vasyunin et al. 2004, 2008; Wakelam et al. 2006, 2010) and observations, one can conclude that this difference is not significant.

Approximately one-third of total methyl formate production belongs to the ion-neutral route that includes the formation of protonated methyl formate via the reaction

$$CH_3OH_2^+ + HCOOH \rightarrow HC(OH)OCH_3^+ + H_2O, \quad (24)$$

with subsequent dissociative recombination into $HCOOCH_3$. Reaction (24) has been turned down in Horn et al. (2004) who cited an older study by Freeman et al. (1978). However, in a recent study by Cole et al. (2012), a 5% probability for the formation of a protonated methyl formate (with the rest 95% probability to form an adduct ion) in reaction (24) has been found. A protonated methyl formate is converted in our model into $HCOOCH_3$ in a dissociative recombination reaction with electrons with a probability of 50%. However, one should note that the latter probability is poorly known and could be much smaller (Vigren et al. 2010), resulting in much lower production of methyl formate by the considered ion-molecular route.

Formic acid (HCOOH), the second reactant in reaction (24), is another brick of organic chemistry in star-forming regions. It has also been detected by Vastel et al. (2014) toward L1544, with a fractional abundance of $\sim 10^{-10}$ wrt. H. In our model, the gas-phase abundance of formic acid toward the location of the "methanol peak" at the time of best agreement ($1.6 \times 10^5$ years) is $2.0 \times 10^{-10}$. HCOOH is formed as a product of dissociative recombination of its protonated form $HCOOH_2^+$, which is, in turn, formed in a slow radiative association reaction $HCO^+ + H_2O \rightarrow HCOOH_2^+ + h\nu$. The surface formation route of formic acid in the reaction between OH and HCO is inefficient because in our model both reactants do not diffuse in the surface at the low temperatures of prestellar cores. Nevertheless, a total abundance of HCOOH of $\sim 7 \times 10^{-9}$ wrt. H is accumulated in the ice via gas accretion. The compilation done by Garrod & Herbst (2006) shows that the observed abundances of HCOOH in hot cores vary in the range of $[8.0 \times 10^{-10}$–$6.2 \times 10^{-8}]$ wrt. H. Thus, assuming that hot core/corino is the next stage in the development of a protostar that inherits the chemical composition from the previous stage, one may deduce that the total production of HCOOH in our model is within reasonable limits.

Nitrogen-bearing COMs with a peptide bond such as formamide ($NH_2CHO$) exhibit a plateau-like abundance profile between 0.01 and 0.05 pc at $10^5$ years, reaching $\sim 6 \times 10^{-12}$ wrt. H (see Figure 8, bottom panel). Formamide in our

model is solely produced via reaction (12) despite the existence of two surface reactions, leading to $NH_2CHO$. Those are s-N+s-$CH_2OH$ → s–$NH_2CHO$ and s–$NH_2$ + s–HCO → s–$NH_2CHO$. At low dust temperatures of ∼10 K, typical for L1544, those reactions are not efficient in our model, because with the adopted diffusion-to-desorption energy ratio $E_b/E_D = 0.55$, the grain surface diffusion timescale even for relatively weakly bound nitrogen atoms exceeds $10^{13}$ years.

Both reactants in reaction (12), $NH_2$ and $H_2CO$, are produced in the gas phase (20% of $NH_2$, 80% of $H_2CO$) and on surface ice, and then ejected non-thermally to the gas. Amidogen ($NH_2$) on the surface is produced in the hydrogenation reaction H + NH → $NH_2$, and in the gas as a product of dissociative recombination of $NH_4^+$. Formaldehyde ($H_2CO$) on the surface is produced in the hydrogenation reaction H + HCO → $H_2CO$, and in the gas phase via the reaction O + $CH_3$ → $H_2CO$ + H. The possible reason why $NH_2CHO$ is somewhat overproduced in our model with respect to the observed upper limit (see Table 3) is due to too high efficiencies of formation of the reactants of the reaction (12). See Section 4 for details.

Acetaldehyde ($CH_3CHO$) is mainly produced in reaction (13). Due to the high rate of this reaction, both temporal and spatial profiles of acetaldehyde are well correlated with those of methanol, and $CH_3CHO$ reaches peak abundances about two orders of magnitude higher than other COMs considered in this study, though at a very early time (see Figure 7). By the time of the best agreement with observations, $1.6 \times 10^5$ years, the abundance of $CH_3CHO$ is within an order of magnitude to those of $HCOOCH_3$ and $CH_3OCH_3$ (see Figures 7 and 8), as well as to its observed value (see Table 3).

This mechanism of formation of acetaldehyde is different from that described in Vasyunin & Herbst (2013b), where acetaldehyde was mainly produced in the gas phase via the neutral–neutral reaction O + $C_2H_5$ → $CH_3CHO$ + H. The reason for this is the updated treatment of RD in the current study. In Vasyunin & Herbst (2013b), $C_2H_5$ is delivered to the gas from the surface via RD. In Vasyunin & Herbst (2013b), all species formed on the surface had a single RD efficiency of 10%, while in the current study, we use expression (7). For the surface reaction s–H + s–$C_2H_4$ → $C_2H_5$, which is the main source of $C_2H_5$ in Vasyunin & Herbst (2013b), expression (7) gives the efficiency of RD 0.0005%, even for the part of the surface consisting of heavy species, i.e., effectively zero. As such, the chemistry of acetaldehyde becomes different in this study in comparison to Vasyunin & Herbst (2013b), and the peak abundance of $CH_3CHO$ in the absence of reaction (13) becomes two orders of magnitude lower than in Vasyunin & Herbst (2013b).

Finally, let us consider the chemistry of methanol in the gas phase in our model of L1544. There are no significant contributions from gas-phase reactions to the formation of methanol. The full amount of methanol is ejected to the gas phase from the surfaces of icy mantles of interstellar grains, where $CH_3OH$ is formed as a product of hydrogenation of the CO molecule (see Section 2.2). The main ejection mechanism is non-thermal RD from the part of the surface covered with "heavy species" (see Figure 6), with an efficiency of 0.64% that matches previous more conservative estimates of RD efficiency (Garrod et al. 2007). Other non-thermal desorption mechanisms (photodesorption and cosmic-ray-induced desorption) do not contribute significantly to the desorption rate of methanol. The main destruction route of methanol in the gas phase is reaction (20), as well as ion-molecule reactions with major ions such as $H_3^+$ and $H_3O^+$. It is important to note that the peak local volume abundances of COMs in our model does not coincide with the peak local volume abundance of methanol (see Figure 8, left lower panel), though due to averaging effects in single-dish observations, the peak abundances of COMs and methanol inferred from column densities spatially coincide near the observed "methanol peak" (see Figure 8, lower right panel). As such, a very high abundance of methanol in the gas phase is not needed to reproduce observed abundances of COMs. Moreover, we attribute the highest abundance of methanol reached in its radial profile ($7 \times 10^{-8}$ wrt. H at $R = 0.04$ pc) to the fact that dynamics is ignored. In a dynamical model, which starts with lower densities, the CO freeze out will be less efficient and, consequently, less $CH_3OH$ is expected to be produced.

### 3.3. The Role of RD in the Chemistry of Cold COMs

Although in our model COMs in the cold environments typical of prestellar cores are formed via gas-phase chemistry, the role of surface chemistry in the formation of precursor species, and of RD for their delivery to the cold gas, is pivotal. To illustrate this, we ran two models with different efficiencies of RD. In the first illustrative model (IM0), RD is switched off (efficiency 0%). In the second illustrative model (IM10), the RD efficiency for all species is 10%, same as in Vasyunin & Herbst (2013b). Best-fit radial profiles of abundances of COMs and their precursors for the illustrative models are shown in Figure 10 for the model with no RD and in Figure 11 for the model with 10%-efficiency RD. In addition, in Table 4, we list the main precursors of COMs in the gas phase, their RD efficiencies and contribution from surface chemistry to the total rate of formation rates of those species in the gas phase in our main model with advanced treatment of RD.

Let us first consider the illustrative model with RD switched off (IM0). As can be seen on the "agreement map" in Figure 9 (left column), in the entire space (time, radius) there is no area where the model matches observational data satisfactorily. As an example, the radial profiles of fractional abundances are plotted in Figure 10 at $8 \times 10^4$ years of evolution, that corresponds to the minimum value of $F(r, t)$ in Equation (17). In model IM0, fractional abundances of all COMs considered in this study do not exceed $10^{-12}$ wrt. H. Note that there are two other types of non-thermal desorption included in all models considered in this study—photodesorption and cosmic-ray-induced desorption. However, it appears that the efficiency of these two other types of non-thermal desorption processes are clearly not high-enough to provide sufficient amounts of precursors of COMs to the cold gas.

The resulting radial profiles of abundances obtained with the second illustrative model (IM10), in which the RD efficiency for all species is set to a single value of 10%, are shown in Figure 11 for the times of the best agreement with observations, which is $3 \times 10^6$ years of cloud evolution. At that time, the modeled CO column density is too low in comparison to the observed value (see Figure 3). As can be seen in Figure 9 (middle column), the illustrative model with 10% efficiency of RD also does not agree with observations in the entire parameter space considered (time, radius). One can see that the peak abundances of COMs in the illustrative model with RD efficiency 10% are significantly higher than in our main

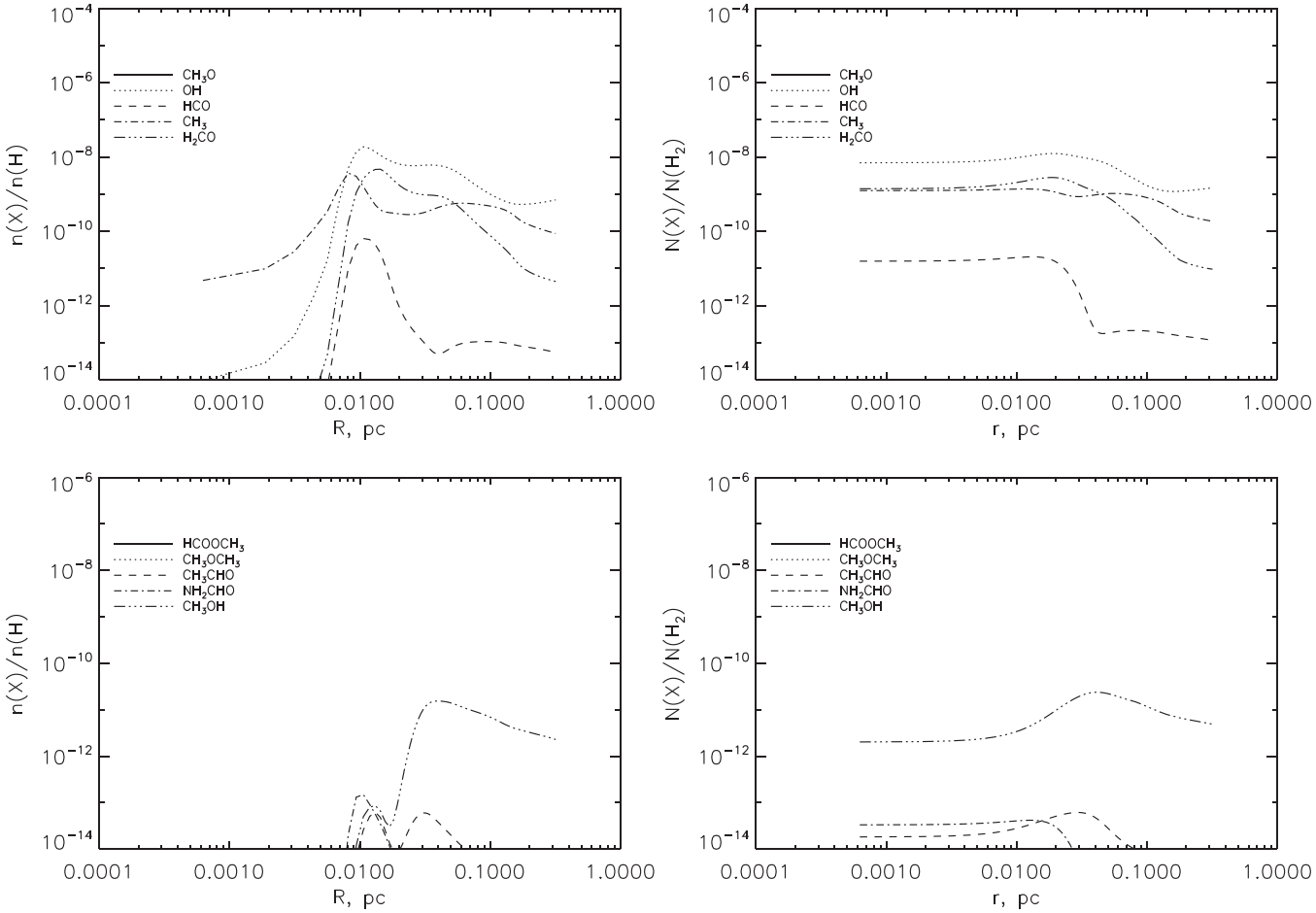


**Figure 10.** Same as in Figure 8, but at $8.0 \times 10^4$ years calculated with reactive desorption completely disabled. $8.0 \times 10^4$ years is the time of the best agreement (minimal $F(r, t)$, see text) between the modeled and observed abundances of species inferred from column densities. New gas-phase chemical reactions are not sufficient to reproduce abundances of COMs without supply of precursor species from grain surface via reactive desorption.

model, with the exception of methyl formate. The peak abundances of COMs are located near $R = 0.04$ pc, which is somewhat inconsistent with the observed location of the "methanol peak" (see Bizzocchi et al. 2014 and Jiménez-Serra et al. 2016). The abundance of acetaldehyde ($CH_3CHO$) is equal to $1.0 \times 10^{-8}$ wrt. H, which is higher than the abundance observed toward the hot core in Sgr B2 (Belloche et al. 2013; Occhiogrosso et al. 2014). Abundances of other species are also higher than in our main model by about an order of magnitude, with the exception of methyl formate, whose abundance drops with time faster than that of other species. In summary, for the majority of species, the IM10 model gives the values of column densities of COMs higher than those obtained with our Main model (MM). Averaged column densities are also higher than observed by one to three orders of magnitude even at the late evolutionary time of $3 \times 10^6$ years. No location is found in the parameter space (time, radius) with satisfactory agreement with observations of COMs in L1544.

## 4. Discussion

Although remarkable progress has been made during the last years, our knowledge of the formation and evolution of organic matter in star-forming regions is still far from being comprehensive. In particular, models of formation of saturated COMs that have been found in cold clouds representing the earliest stages of star formation (Öberg et al. 2010; Bacmann et al. 2012; Cernicharo et al. 2012; Vastel et al. 2014), are under active development. As such, certain controversy exists between the models and adopted physical parameters. The Main model (MM) presented in this work, is a development of the model proposed in Vasyunin & Herbst (2013b), but it differs in treatment of RD, in the adopted set of gas-phase reactions and in the utilized parameters of surface chemistry. It is important to assess the importance of introduced changes, to compare the proposed model with others available, and to discuss the issues that exist in the model.

In contrast to Vasyunin & Herbst (2013b), where grain surface chemistry was treated in a simplistic way without taking into account the ice thickness, in the current study, we use a multilayer approach to the chemistry on interstellar grains. Under the conditions of prestellar cores, icy mantles can reach thickness up to several hundreds of monolayers, while accumulating over large periods of time. Therefore, it is reasonable to distinguish between surface layers of ice, where the fast diffusive chemistry occurs as well as thermal and non-thermal desorption, and the inner parts of icy mantles, which may have different composition, and conditions for chemistry to occur. Following Fayolle et al. (2011) and Vasyunin & Herbst (2013a), four upper layers of the ice in our model comprise the "surface ice." Because, according to our model, the total ice thickness in the central dark region of L1544

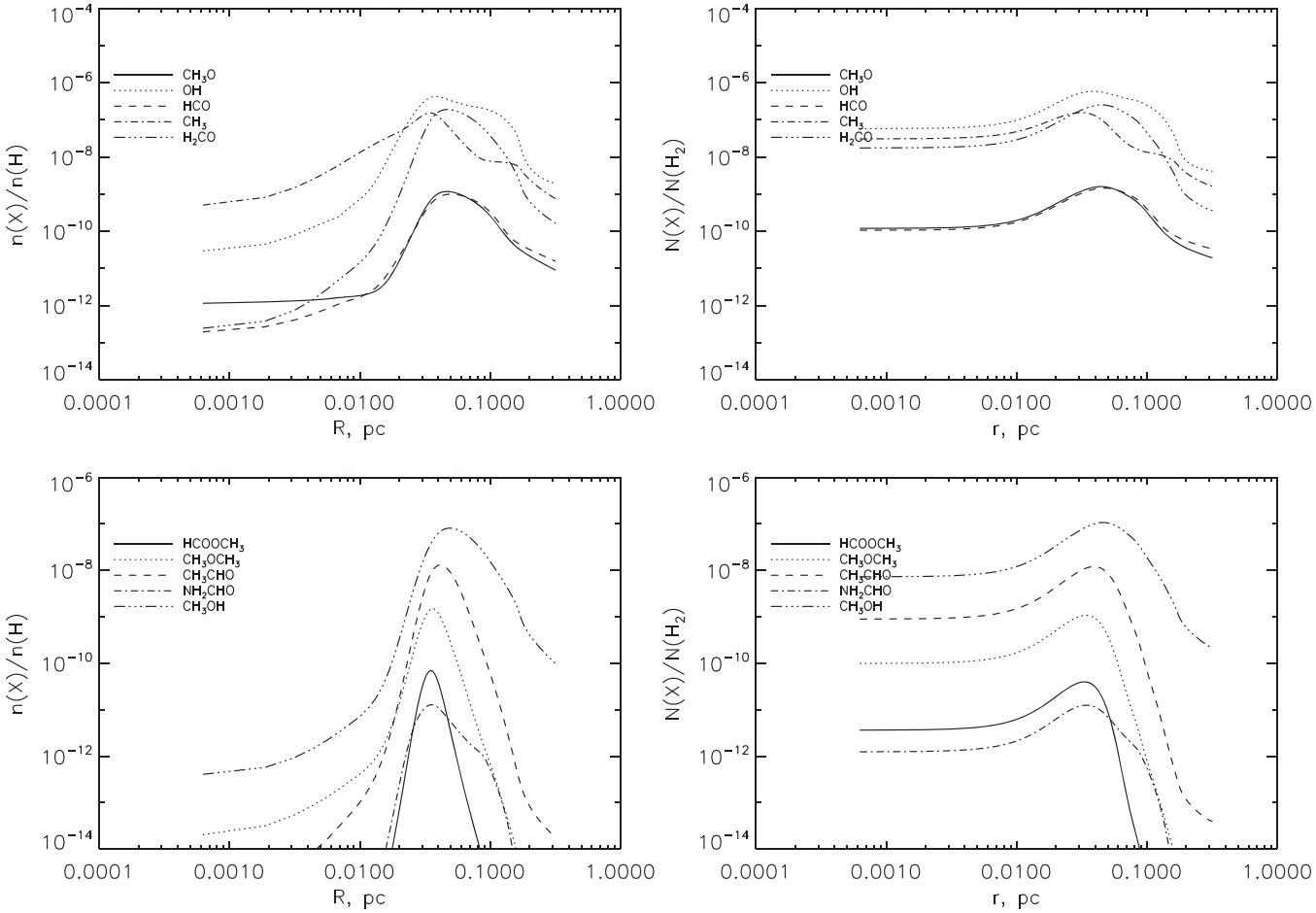


**Figure 11.** Same as in Figure 8, but at $3.0 \times 10^6$ years calculated with single 10% efficiency of reactive desorption. $3.0 \times 10^6$ years is the time of the best agreement (minimal $F(r, t)$, see the text) between the modeled and observed abundances of species inferred from column densities.

**Table 4**
Key Gas-phase Precursors of COMs, and Contribution from Surface Chemistry to Their Total Formation Rate at the Moment of Best Agreement at $R = 0.015$ pc in Main Model (MM)

| Species | Surface Contribution, % | RD Efficiency |
|---|---|---|
| $CH_3O$ | 45 | 3.4(−5) |
| OH | 10 | 4.5(−2) |
| HCO | 20 | 2.1(−3) |
| $CH_3$ | 3 | 6.2(−1) |
| $C_2H_4$ | 98 | 6.0(−2) |
| $NH_2$ | 5 | 2.5(−1) |
| $H_2CO$ | 75 | 5.4(−2) |
| $CH_3OH$ | 99 | 6.4(−3) |

exceeds 200 monolayers, only a few percent of atoms and molecules residing on grains are available to participate in reactions on surface ice and to be ejected to the gas via RD. This is in contrast to Vasyunin & Herbst (2013b), where all species on grains were available for these processes. Effectively, it means that rates of reactions causing RD in our updated model are generally smaller due to a smaller number of available reactants. As such, while in Vasyunin & Herbst (2013b), the best-fit model has only thermal hopping as a source of diffusion of species on the surface, in this study, we had to enable quantum tunneling for H and $H_2$ in order to ensure sufficient rates of reactions in surface layers of ice, and thus rates of RD. Therefore, our updated model with the multilayer approach to ice chemistry, and advanced treatment of RD based on Minissale et al. (2016b), requires efficient quantum tunneling for H and $H_2$ to reproduce the COM observations by Jiménez-Serra et al. (2016) toward L1544. With tunneling for diffusion enabled, at the low temperature of ∼10 K, the exact value of another poorly known parameter that controls surface chemistry, diffusion-to-desorption energy ratio, becomes unimportant.

Another key assumption in this study, is the high efficiency of RD from the fraction of surface ice covered by species with molecular masses higher than those of water. The two most abundant heavy species in this study are carbon monoxide (CO) and methanol ($CH_3OH$). They have similar molecular masses about twice higher than the mass of the water molecule. Near the location of the "methanol peak" in L1544, these two molecules comprise about 50% of the surface ice composition in the Main model (MM). Here, the importance of the multilayer approach to ice chemistry is revealed: while the bulk of ice is dominated by water, the surface layers of ice in a prestellar core are apolar, and covered with CO and methanol, which is in line with ice observations (Öberg et al. 2011). While the high efficiency of RD in certain chemical reactions on bare olivine surface was confirmed experimentally (Dulieu et al. 2013), as well as that water ice surface severely reduces the efficiency of RD (Congiu et al. 2009; Minissale et al. 2016b), to the best of our knowledge, there are no experimental

studies of the efficiency of RD on CO and methanol ices. As such, while our assumption of higher RD efficiency from surface covered with heavy molecules (in comparison to water molecules) looks reasonable to us, it definitely requires experimental confirmation. Interestingly, in a recent study, Wakelam et al. (2017) argues that binding energies of species to water surface are generally higher than it was believed. This may further inhibit the efficiency of RD of species from water ice. However, conclusions made by Wakelam et al. (2017) clearly do not affect results presented in the current study, since we only assume efficient RD from non-water fraction of ice surface.

It is also worth noting that the efficiency of RD in our study is determined by expression (7), which is semi-empirical in nature, and is derived based on a limited set of experiments. Expression (7) gives a wide range of RD efficiencies depending on a particular reaction and on reactants. In this study, expression (7) is also applied to systems not studied experimentally. Also, one should bear in mind that in case of certain species, expression (7) includes poorly known parameters. For example, to the best of our knowledge, the binding energy of $NH_2$ has never been measured. Thus, the adopted value of desorption energy for $NH_2$ of 3960 K may be too low, leading to the too high efficiency of RD according to (7), which is equal to 25% (see Table 4). This may lead to the marginally overestimated abundance of $NH_2CHO$ in our model over the upper limit set by the observations of Jiménez-Serra et al. (2016). On the other hand, the fractional abundance of $NH_2$ in our Main model (MM) at $10^5$ years is $1.5 \times 10^{-10}$ wrt. H, which is consistent with the model of Le Gal et al. (2014). Moreover, the $NH_2$:$NH_3$ ratio in our Main model (MM) is close to 1:20, which is also consistent with Le Gal et al. (2014). Therefore, the overproduction of gas-phase $H_2CO$ seems to be the most probable reason for the slight overproduction of $NH_2CHO$.

While non-thermal RD in our model is a key process that delivers precursors of COMs to the cold gas, the COMs themselves are formed via gas-phase chemical reactions. During the last decade, the long-standing paradigm of astrochemistry stating that the most important reactions in the cold ISM are ion-molecule reactions, has been somewhat changed. Since Smith et al. (2004), it has been recognized that fast neutral–neutral reactions can affect the abundances of exotic carbon-bearing species in cold clouds. Vasyunin & Herbst (2013b) proposed that reactions of radiative association may be important for the formation of some terrestrial-type organic molecules such as dimethyl ether. However, the majority of gas-phase reactions responsible for the formation of COMs in Vasyunin & Herbst (2013b) are ion-molecule reactions leading to the formation of protonated COMs that must recombine with electrons in order to form neutral species. This scheme is somewhat problematic because the outcome of neutral COMs in the recombination process is not clear.

In this study, gas-phase chemistry of COMs has more solid basis thanks to theoretical and experimental studies during the last years. The chemical link between $CH_3OCH_3$ and $HCOOCH_3$ via the intermediate species $CH_3OCH_2$ proposed in Balucani et al. (2015), solves the problem of underproduction of methyl formate via the ion-molecule route discussed in Vasyunin & Herbst (2013b). However, it is worth noting that in our study, $CH_3OCH_2$ is formed via reaction (9), which is proposed in Shannon et al. (2014), but missing in Balucani et al. (2015). Reactions with chlorine and fluorine in our model cannot produce sufficient amounts of $CH_3OCH_2$ due to strong depletion of Cl and F in the cold gas. As such, it is not entirely clear to us how the model by Balucani et al. (2015) works in the presented form.

As shown in Section 3.2, the mechanism of formation of $CH_3CHO$ discussed in Vasyunin & Herbst (2013b) is not working in the updated model due to the new description of RD. As such, new chemical pathways to acetaldehyde in the cold gas should be considered. In this work, we included reaction (13) as one of the possible efficient routes to form acetaldehyde in the cold gas. It is interesting to note that methylidyne radical (CH) has a certain similarity of chemical properties with the hydroxyl radical (OH). The enhanced rates of gas-phase reactions with hydroxyl radical (OH) found by Shannon et al. (2013, 2014) are shown to impact chemistry of COMs in cold gas. Thus, it may be reasonable to expect that reactions with methylidyne radical could have a broader impact on the chemistry of COMs than currently assessed and are worth further detailed studies. Another reaction to form $CH_3CHO$ proposed in this work is the radiative association reaction (16). We propose this reaction by analogy with reaction (18), which is currently considered to be a major route of the formation of dimethyl ether (Cernicharo et al. 2012; Vasyunin & Herbst 2013b; Balucani et al. 2015). However, one should point out that, to the best of our knowledge, reaction (16) has not been studied under the conditions relevant to cold molecular clouds.

It is worth noting a surprisingly good agreement between the results produced by our complex and uncertain multiparameter chemical model, and the observational data presented in Jiménez-Serra et al. (2016). Also, at the time of best agreement with observations ($\sim 10^5$ years), our model reproduces reasonably well the abundance ratios for COMs-related species (with the exception of formaldehyde) observed by Bacmann & Faure (2016) in other prestellar cores. Namely, they found the ratios for $HCO:H_2CO:CH_3O:CH_3OH \sim 10:100:1:100$. As can be seen in Table 3, our modeled ratios are 5:480:1:270. Since the sample of prestellar cores by Bacmann & Faure (2016) does not include L1544, it is not clear if the reason for the disagreement belongs to deficiency of our model, or to the different physical structure.

Possible problems in our chemical model include overproduction of gas-phase formaldehyde and methanol. As noted above, this may be caused by possibly overestimated efficiency of RD of $H_2CO$ and $CH_3OH$ with the expression (7) that is semi-empirical in nature and includes poorly known values. However, as can be seen in Table 4, RD efficiencies for these species are not extremely high (0.64% for $CH_3OH$ and 5.4% for $H_2CO$), which is consistent with conservative estimates of RD efficiencies (e.g., Garrod et al. 2007). Another possible reason for the too high abundances of methanol and formaldehyde in the gas phase in our model is their overproduction on grains that is translated into gas via RD, which also leads to the somewhat increased fractions of $CH_3OH$ and $H_2CO$ in the ice bulk (see lower panel of Figure 5, Table 2) as compared to observed values (Öberg et al. 2011). One possible remedy for this is to take into account an evolutionary model for L1544, where dust temperature changes during collapse from typical values for diffuse clouds (of $\sim$20 K) to $\leqslant$10 K (see Vasyunin & Herbst 2013a). This will ensure the formation of another major ice constituent, $CO_2$,

which is currently missing in our static model of L1544. Formation of $CO_2$ will lock 10%–20% of the total carbon budget, thus reducing, among others, the abundances of $H_2CO$ and $CH_3OH$. The formation efficiency of $H_2CO$ and $CH_3OH$ may also be reduced by considering the new scenario that includes backward hydrogen abstraction reactions (Minissale et al. 2016c).

Although in this study we use a time-dependent chemical model, the adopted physical model of L1544 is static. Since timescales of chemical and dynamical evolution of prestellar cores are comparable, a more realistic approach should include a dynamical model of the physical structure of L1544. In fact, the inclusion of dynamical evolution could imply a longer timescale spent by the core at lower volume densities, thus with longer freeze out timescales (because the freeze out timescale is inversely proportional to the volume density). The inclusion of dynamics will be the subject of our next paper. The possible longer freeze-out times in a dynamical model may affect chemistry in the center of the core, where with the current model, an extreme freeze-out of virtually all species is observed, including nitrogen-bearing (see Figure 4), which is somewhat inconsistent with observations. However, another possible explanation for the "extra" depletion of N-bearing molecules could be that the multilayer treatment overestimates the amount of $N_2$ freeze-out (see also Sipilä et al. 2016), so that further laboratory studies will be needed to put more stringent constraints on the mobility of species in the bulk and surfaces of icy mantles.

## 5. Summary

In this study, we performed chemical modeling of the formation and evolution of COMs in the prestellar core L1544. We found that saturated COMs can be formed efficiently in L1544 up to the fractional abundances of the $(3–4) \times 10^{-10}$ wrt. total number of hydrogen nuclei via the scenario proposed in Vasyunin & Herbst (2013b), and further developed in this study. The development includes more detailed treatment of the RD based on experiments by Dulieu et al. (2013) and Minissale et al. (2016b), and an extended set of gas-phase reactions, important for the formation of COMs in the cold gas. Chemistry on interstellar grains is treated via a multilayer approach, which allows us to discriminate between surface and bulk ice. Abundances of many COMs such as $CH_3OCH_3$, $HCOOCH_3$ and $NH_2CHO$ peak at a similar radial distance of 2000–4000 au from the core center, which is in line with recent observations of L1544 performed by Jiménez-Serra et al. (2016), Bizzocchi et al. (2014), and Vastel et al. (2014). Gas-phase abundances of COMs depend on the efficiency of RD, which in turn depends on the composition of the outer monolayers of icy mantles. In prestellar cores, outer monolayers of icy mantles likely include a large fraction of CO and products of CO hydrogenation with atomic weights higher than that of water, which may allow the increase of the efficiency of RD in comparison to that on water ice. As such, the combination of non-thermal desorption and extended gas-phase chemistry based on recent experimental and laboratory works, provides a reasonable explanation for the observed abundances of COMs in L1544, and, probably, in other similar objects.

We believe that a three-phase approach (gas–ice surface–ice bulk) to gas-grain chemistry in star-forming regions should be preferred in modeling over the two-phase approach (gas–ice) even considering all the uncertainties that currently exist in our understanding of the processes on the ice surface and within the ice. The three-phase approach reflects the fundamental fact that dynamics of chemical processes on a solid surface and within the solid body are different, and allows us to explore the astrochemical importance of this fact. While currently three-phase models include more poorly known parameters than two-phase ones, this will change with time with the advent of new experimental and theoretical studies.

The chemical model employed in this study, has revealed the key role of the hydroxyl radical (OH) in the chemistry of several important COMs—methoxy radical, dimethyl ether, and methyl formate. To date, the potential importance of this species for the chemistry of COMs is not fully recognized in the literature. To the best of our knowledge, the only systematic study of OH in prestellar cores has been performed by Harju et al. (2000). Given the importance of the hydroxyl radical for the chemistry of COMs, as well as the possible high efficiency of the entire class of neutral–neutral reactions with OH at low temperatures (Shannon et al. 2013, 2014), we believe that the OH radical is an important target for future observational studies.

Finally, it is important to point out that in this study, we used several important parameters that require more accurate experimental or theoretical measurements. The key assumption of this study—the efficient RD from the surface made of CO and its hydrogenation products—is to be checked in the lab. The binding energy of $NH_2$, a key parameter that influences the abundance of gas-phase formamide in our model, also requires an experimental measurement. Another possible follow-up study is to determine the spectroscopy of $CH_3OCH_2$, which is an intermediate product in the formation of methyl formate. If this intermediate product will be found observationally, it would confirm that this is the main formation route of methyl formate in the gas phase. Experimental or/and theoretical studies of the processes mentioned above, will be an important step in improving our knowledge of the chemistry of COMs in prestellar cores.

This research has made use of NASA's Astrophysics Data System. A.V. and P.C. acknowledge support from the European Research Council (ERC; project PALs 320620). I.J.-S. acknowledges the financial support received from the STFC through an Ernest Rutherford Fellowship (proposal number ST/L004801/1). The authors are thankful to Prof. Eric Herbst for a careful reading and valuable suggestions on the paper, to Dr. Patrice Theulé, Dr. Jean-Christophe Loison and to, Dr. Miwa Goto for the valuable discussions, and to the anonymous referee for the valuable comments that helped to improve the manuscript.

## References

Antinolo, M., Agundez, M., Jimenez, E., et al. 2016, ApJ, 823, 25
Bacmann, A., & Faure, A. 2016, A&A, 587, A130
Bacmann, A., García-García, E., & Faure, A. 2016, A&A, 588, L8
Bacmann, A., Taquet, V., Faure, A., Kahane, C., & Ceccarelli, C. 2012, A&A, 541, L12
Balucani, N., Ceccarelli, C., & Taquet, V. 2015, MNRAS, 449, L16
Barone, V., Latouche, C., Skouteris, D., et al. 2015, MNRAS, 453, L31
Belloche, A., Müller, H. S. P., Menten, K. M., Schilke, P., & Comito, C. 2013, A&A, 559, A47
Bertin, M., Romanzin, C., Doronin, M., et al. 2016, ApJL, 817, L12
Bizzocchi, L., Caselli, P., Spezzano, S., & Leonardo, E. 2014, A&A, 569, A27
Blake, G. A., Sutton, E. C., Masson, C. R., & Phillips, T. G. 1987, ApJ, 315, 621

Bottinelli, S., Ceccarelli, C., Lefloch, B., et al. 2004a, ApJ, 615, 354
Bottinelli, S., Ceccarelli, C., Neri, R., et al. 2004b, ApJL, 617, L69
Callear, A. B., & Cooper, I. A. 1990, J. Chem. Soc., Faraday Trans., 86, 1763
Caselli, P., Walmsley, C. M., Tafalla, M., Dore, L., & Myers, P. C. 1999, ApJL, 523, L165
Caselli, P., Walmsley, C. M., Zucconi, A., et al. 2002, ApJ, 565, 344
Cazaux, S., Tielens, A. G. G. M., Ceccarelli, C., et al. 2003, ApJL, 593, L51
Cernicharo, J., Marcelino, N., Roueff, E., et al. 2012, ApJL, 759, L43
Chang, Q., & Herbst, E. 2016, ApJ, 819, 145
Cole, C. A., Wehres, N., Yang, Z., et al. 2012, ApJL, 754, L5
Congiu, E., Matar, E., Kristensen, L. E., Dulieu, F., & Lemaire, J. L. 2009, MNRAS, 397, L96
Cruz-Diaz, G. A., Martín-Doménech, R., Muñoz Caro, G. M., & Chen, Y.-J. 2016, A&A, 592, A68
Dartois, E., Augé, B., Boduch, P., et al. 2015, A&A, 576, A125
de Graauw, T., Whittet, D. C. B., Gerakines, P. A., et al. 1996, A&A, 315, L345
Dulieu, F., Congiu, E., Noble, J., et al. 2013, NatSR, 3, 1338
Fayolle, E. C., Bertin, M., Romanzin, C., et al. 2011, ApJL, 739, L36
Freeman, C. G., Harland, P. W., & McEwan, M. J. 1978, IJMSI, 28, 377
Fuchs, G. W., Cuppen, H. M., Ioppolo, S., et al. 2009, A&A, 505, 629
Garrod, R., Park, I. H., Caselli, P., & Herbst, E. 2006, FaDi, 133, 51
Garrod, R. T. 2008, A&A, 491, 239
Garrod, R. T. 2013, ApJ, 765, 60
Garrod, R. T., & Herbst, E. 2006, A&A, 457, 927
Garrod, R. T., & Pauly, T. 2011, ApJ, 735, 15
Garrod, R. T., Vasyunin, A. I., Semenov, D. A., Wiebe, D. S., & Henning, T. 2009, ApJL, 700, L43
Garrod, R. T., Wakelam, V., & Herbst, E. 2007, A&A, 467, 1103
Garrod, R. T., Weaver, S. L. W., & Herbst, E. 2008, ApJ, 682, 283
Gibb, E. L., Whittet, D. C. B., Boogert, A. C. A., & Tielens, A. G. G. M. 2004, ApJS, 151, 35
Gillett, F. C., & Forrest, W. J. 1973, ApJ, 179, 483
Grim, R. J. A., Baas, F., Greenberg, J. M., Geballe, T. R., & Schutte, W. 1991, A&A, 243, 473
Hama, T., & Watanabe, N. 2013, ChRv, 113, 8783
Harju, J., Winnberg, A., & Wouterloot, J. G. A. 2000, A&A, 353, 1065
Hasegawa, T. I., & Herbst, E. 1993, MNRAS, 261, 83
Hasegawa, T. I., Herbst, E., & Leung, C. M. 1992, ApJS, 82, 167
Hayes, W. W., Oh, J., Kondo, T., et al. 2012, JPCM, 24, 104010
He, J., Jing, D., & Vidali, G. 2014, PCCP, 16, 3493
Herbst, E., & van Dishoeck, E. F. 2009, ARA&A, 47, 427
Horn, A., Møllendal, H., Sekiguchi, O., et al. 2004, ApJ, 611, 605
Hoyermann, K., & Nacke, F. 1996, Symposium (International) on Combustion, 26, 505
Husain, D., & Ioannou, A. X. 1999, Journal of Photochemistry and Photobiology A: Chemistry, 129, 1
Ivlev, A. V., Röcker, T. B., Vasyunin, A., & Caselli, P. 2015, ApJ, 805, 59
Jiménez-Serra, I., Vasyunin, A. I., Caselli, P., et al. 2016, ApJL, 830, L6
Johnson, D. G., Blitz, M. A., & Seakins, P. W. 2000, PCCP, 2, 2549
Keto, E., & Caselli, P. 2010, MNRAS, 402, 1625
Lacy, J. H., Baas, F., Allamandola, L. J., et al. 1984, ApJ, 276, 533
Lacy, J. H., Carr, J. S., Evans, N. J., II, et al. 1991, ApJ, 376, 556
Le Gal, R., Hily-Blant, P., Faure, A., et al. 2014, A&A, 562, A83
Marcelino, N., Cernicharo, J., Roueff, E., Gerin, M., & Mauersberger, R. 2005, ApJ, 620, 308
McElroy, D., Walsh, C., Markwick, A. J., et al. 2013, A&A, 550, A36
Mennella, V., Baratta, G. A., Palumbo, M. E., & Bergin, E. A. 2006, ApJ, 643, 923
Minissale, M., Congiu, E., Baouche, S., et al. 2013, PhRvL, 111, 053201
Minissale, M., Congiu, E., & Dulieu, F. 2016a, A&A, 585, A146
Minissale, M., & Dulieu, F. 2014, JChPh, 141, 014304
Minissale, M., Dulieu, F., Cazaux, S., & Hocuk, S. 2016b, A&A, 585, A24
Minissale, M., Moudens, A., Baouche, S., Chaabouni, H., & Dulieu, F. 2016c, MNRAS, 458, 2953
Muñoz Caro, G. M., Dartois, E., Boduch, P., et al. 2014, A&A, 566, A93
Öberg, K. I., Boogert, A. C. A., Pontoppidan, K. M., et al. 2011, ApJ, 740, 109
Öberg, K. I., Bottinelli, S., Jørgensen, J. K., & van Dishoeck, E. F. 2010, ApJ, 716, 825
Öberg, K. I., van Dishoeck, E. F., & Linnartz, H. 2009, A&A, 496, 281
Occhiogrosso, A., Vasyunin, A., Herbst, E., et al. 2014, A&A, 564, A123
Pontoppidan, K. M., van Dishoeck, E. F., & Dartois, E. 2004, A&A, 426, 925
Prasad, S. S., & Tarafdar, S. P. 1983, ApJ, 267, 603
Reboussin, L., Wakelam, V., Guilloteau, S., & Hersant, F. 2014, MNRAS, 440, 3557
Ruaud, M., Loison, J. C., Hickson, K. M., et al. 2015, MNRAS, 447, 4004
Ruaud, M., Wakelam, V., & Hersant, F. 2016, MNRAS, 459, 3756
Ruffle, D. P., & Herbst, E. 2001, MNRAS, 322, 770
Sandford, S. A., Bernstein, M. P., Allamandola, L. J., Goorvitch, D., & Teixeira, T. C. V. S. 2001, ApJ, 548, 836
Shannon, R. J., Blitz, M. A., Goddard, A., & Heard, D. E. 2013, NatCh, 5, 745
Shannon, R. J., Caravan, R. L., Blitz, M. A., & Heard, D. E. 2014, PCCP, 16, 3466
Sipilä, O., Caselli, P., & Taquet, V. 2016, A&A, 591, A9
Skouteris, D., Vazart, F., Ceccarelli, C., et al. 2017, arXiv:1701.06138
Smith, I. W. M., Herbst, E., & Chang, Q. 2004, MNRAS, 350, 323
Song, X., Hou, H., & Wang, B. 2005, PCCP, 7, 3980
Tafalla, M., Myers, P. C., Caselli, P., & Walmsley, C. M. 2004, A&A, 416, 191
Tafalla, M., Myers, P. C., Caselli, P., Walmsley, C. M., & Comito, C. 2002, ApJ, 569, 815
Taquet, V., Ceccarelli, C., & Kahane, C. 2012, A&A, 538, A42
Taquet, V., Peters, P. S., Kahane, C., et al. 2013, A&A, 550, A127
Tielens, A. G. G. M., Tokunaga, A. T., Geballe, T. R., & Baas, F. 1991, ApJ, 381, 181
van Dishoeck, E. F. 2004, ARA&A, 42, 119
van Dishoeck, E. F., Jonkheid, B., & van Hemert, M. C. 2006, FaDi, 133, 231
Vastel, C., Ceccarelli, C., Lefloch, B., & Bachiller, R. 2014, ApJL, 795, L2
Vastel, C., Ceccarelli, C., Lefloch, B., & Bachiller, R. 2016, A&A, 591, L2
Vasyunin, A. I., & Herbst, E. 2013a, ApJ, 762, 86
Vasyunin, A. I., & Herbst, E. 2013b, ApJ, 769, 34
Vasyunin, A. I., Semenov, D., Henning, T., et al. 2008, ApJ, 672, 629
Vasyunin, A. I., Sobolev, A. M., Wiebe, D. S., & Semenov, D. A. 2004, AstL, 30, 566
Vigren, E., Hamberg, M., Zhaunerchyk, V., et al. 2010, ApJ, 709, 1429
Wakelam, V., & Herbst, E. 2008, ApJ, 680, 371
Wakelam, V., Herbst, E., Le Bourlot, J., et al. 2010, A&A, 517, A21
Wakelam, V., Herbst, E., & Selsis, F. 2006, A&A, 451, 551
Wakelam, V., Loison, J.-C., Herbst, E., et al. 2015, ApJS, 217, 20
Wakelam, V., Loison, J.-C., Mereau, R., & Ruaud, M. 2017, MolAs, 6, 22
Wallington, T. J., Skewes, L. M., Siegl, W. O., Wu, C.-H., & Japar, S. M. 1988, International Journal of Chemical Kinetics, 20, 867